Available online at www.sciencedirect.com
ScienceDirect
Journal of Volcanology and Geothermal Research 159 (2007) 366–392
Journal of volcanology and geothermal research
www.elsevier.com/locate/jvolgeores

Adakitic magmas in the Ecuadorian Volcanic Front: Petrogenesis of the Iliniza Volcanic Complex (Ecuador)

Silvana Hidalgo [a,b,*], Michel Monzier [c,b,✠], Hervé Martin [b], Gilles Chazot [b], Jean-Philippe Eissen [c,b], Jo Cotten [d]

[a] *Departamento de Geofísica, Escuela Politécnica Nacional, Ap. 17-01-2759, Quito, Ecuador*
[b] *Laboratoire Magmas et Volcans, UMR 6524, Université Blaise Pascal, 5 rue Kessler, 63038 Clermont-Ferrand cedex, France*
[c] *IRD, UR 163, 5 rue Kessler, 63038 Clermont-Ferrand cedex, France*
[d] *UMR 6538, Université de Bretagne Occidentale, BP 809, 29285 Brest cedex, France*

Received 25 November 2004; received in revised form 3 January 2006; accepted 18 July 2006
Available online 25 October 2006

Abstract

The Iliniza Volcanic Complex (IVC) is a poorly known volcanic complex located 60 km SSW of Quito in the Western Cordillera of Ecuador. It comprises twin peaks, North Iliniza and South Iliniza, and two satellite domes, Pilongo and Tishigcuchi. The study of the IVC was undertaken in order to better constrain the role of adakitic magmas in the Ecuadorian arc evolution. The presence of volcanic rocks with an adakitic imprint or even pristine adakites in the Ecuadorian volcanic arc is known since the late 1990s. Adakitic magmas are produced by the partial melting of a basaltic source leaving a garnet rich residue. This process can be related to the melting of an overthickened crust or a subducting oceanic crust. For the last case a special geodynamic context is required, like the subduction of a young lithosphere or when the subduction angle is not very steep; both cases are possible in Ecuador. The products of the IVC, made up of medium-K basaltic andesites, andesites and dacites, have been divided in different geochemical series whose origin requires various interactions between the different magma sources involved in this subduction zone. North Iliniza is a classic calc-alkaline series that we interpret as resulting from the partial melting of the mantle wedge. For South Iliniza, a simple evolution with fractional crystallization of amphibole, plagioclase, clinopyroxene, magnetite, apatite and zircon from a parental magma, being itself the product of the mixing of 36% adakitic and 64% calc-alkaline magma, has been quantified. For the Santa Rosa rhyolites, a slab melting origin with little mantle interactions during the ascent of magmas has been established. The Pilongo series magma is the product of a moderate to high degree (26%) of partial melting of the subducting oceanic crust, which reached the surface without interaction with the mantle wedge. The Tishigcuchi series shows two stages of evolution: (1) metasomatism of the mantle wedge peridotite by slab melts, and (2) partial melting (10%) of this metasomatized source. Therefore, the relative ages of the edifices show a geochemical evolution from calc-alkaline to adakitic magmas, as is observed for several volcanoes of the Ecuadorian arc.
© 2006 Elsevier B.V. All rights reserved.

Keywords: Volcanic complex; geochemistry; LA-ICP-MA; metasomatism; adakites; Ecuador; NVZ

1. Introduction

Subduction zones consist in complex tectono-magmatic domains where at least 4 components play a role in

* Corresponding author.
E-mail address: s.hidalgo@opgc.univ-bpclermont.fr (S. Hidalgo).
✠ Deceased.

0377-0273/$ - see front matter © 2006 Elsevier B.V. All rights reserved.
doi:10.1016/j.jvolgeores.2006.07.007

magma genesis: (1) the subducted basaltic oceanic crust, whose age and degree of alteration can widely vary; (2) the subducted sediments, when available; (3) the mantle wedge, and (4) either oceanic or continental arc crust. Whatever is the role played by each component, the subducted oceanic crust always participate in magma genesis either (1) by providing dehydration fluids that induce melting of the overlying mantle wedge, or (2) by direct, fluid present, slab melting.

At the beginning of plate tectonics theory, magma genesis in volcanic arcs was explained by direct partial melting of the subducted oceanic crust (Ringwood, 1974; Wyllie and Sekine, 1982). Later, due to constraints provided by experimental petrology and geochemistry, it has been proposed that calc-alkaline magmas were produced by partial melting of mantle wedge peridotite, previously metasomatized by hydrous fluids released from the subducted slab (Tatsumi, 1986, 1989; Tatsumi and Eggins, 1995; Tatsumi and Kogiso, 1997; Schmidt and Poli, 1998). However, the slab-melting hypothesis has been reinforced by the recognition of a particular kind of volcanic rocks, first in Adak Island (Kay, 1978) and afterwards in some other volcanic arcs (Martin, 1987; Drummond and Defant, 1990; Sajona et al., 1993; Maury et al., 1996; Martin et al., 2005). These unusual volcanic rocks, called *adakites* (Defant and Drummond, 1990; Drummond and Defant, 1990), are characterized by $SiO_2 > 56\%$, low K, high Al (>15% Al_2O_3 at 70% SiO_2), high Na and Sr (>400 ppm) and by very low Y and HREE contents. The mineralogical phases present in these rocks are mainly plagioclase, hornblende and biotite; pyroxenes are rare but may be also present (Maury et al., 1996). Accessory phases are apatite, zircon, sphene and titanomagnetite (see Martin et al., 2005 for review). Modern adakite magmatism is apparently restricted to where a young and relatively hot oceanic crust (Defant et al., 1992; Maury et al., 1996; Sajona et al., 1996; Stern and Killian, 1996), or an active spreading center (Lagabrielle et al., 1994. Sigmarsson et al., 1998) is subducted. Adakites have also been recognized in relation with asthenosphere tears (Yogodzinski et al., 2001). Nevertheless, an alternative hypothesis to produce adakitic geochemical characteristics considers melting of the lower arc crust (Kilian et al., 1995; Petford and Atherton, 1996; Petford and Gallagher, 2001; Annen and Sparks, 2002). In this work we will use the term calc-alkaline magma for the magmas produced by the partial melting of the hydrous metasomatized peridotite from the mantle wedge without involvement of slab melts, while pristine adakite will refer to the magmas produced by the partial melting of a basaltic source without strong evidences of mantle interactions. It must be noted that the calc-alkaline magmas can evolve through fractional crystallization thus leading to the Basalt–Andesite–Dacite–Rhyolite (BADR) suite (Defant and Drummond, 1990).

The presence of volcanic rocks with an adakitic signature or even of pristine adakites (SiO_2 between 63 and 70 wt.%, Na_2O (>3.5%) and by very low Y (<18 ppm) and HREE concentrations) has been recognized in the Ecuadorian volcanic arc since the last decade (Monzier et al., 1997; Bourdon, 1999; Beate et al., 2001; Samaniego, 2001; Bourdon et al., 2002a,b, 2003; Samaniego et al., 2002; Samaniego et al., 2005). In Ecuador, volcanism is related to the subduction of the Nazca Plate (12–22 My in age; Lonsdale, 1978), at an average rate of 58 mm yr^{-1} and with an almost E–W direction (Trenkamp et al., 2002), beneath the North Andean Block, an independent micro plate located in the North Western part of South America (Pennington, 1981; Kellogg et al., 1985). The young Nazca Plate includes the Carnegie Ridge, which results from the Galapagos hot spot activity. Subduction of such a ridge must certainly modify the physical and thermal parameters of the subduction zone. For instance, several authors (Gutscher et al., 1999, 2000; Bourdon et al., 2003) consider that, due to its young age, the Carnegie ridge is warmer and has a lower density than the surrounding Nazca plate. The resulting buoyancy of the ridge contributes to increase the local buoyancy of the Nazca plate itself, which, according to these authors, produces an ongoing flat slab configuration under the Ecuadorian Arc. In such conditions, the subducted slab would remain under P–T conditions allowing its partial melting during a long period of time (Gutscher et al., 2000). However, if slab geometry beneath Ecuador volcanic arc may not be well constrained by ISC (International Seismological Centre) or NEIC (National Earthquake Information Center) data (Pennington, 1981; Gutscher et al., 1999), recent data from a local network (Guillier et al., 2001) unambiguously show that a flat slab configuration does not exist today beneath Ecuador, indicating a Wadatti–Benioff Zone that dips with angles between about 35° in the north to about 25° in the south. Nevertheless, the slab dip is less steep beneath Ecuador than it is, for instance, beneath Colombia (Gutscher et al., 1999; Bourdon et al., 2003), indicating a depth of about 100–120 km for the slab under the volcanic front, which well agrees with the depths at which a young basaltic crust could melt (Peacock et al., 1994). In addition, the lack of strong intermediate seismicity shown by ISC or NEIC data indicates that the subducted plate does not behave as a brittle structure, which could be due to its

high temperature and could also be caused by the fact that it could be partially molten (Morris, 1995).

The Iliniza Volcanic Complex (IVC) is located on the Ecuadorian Volcanic Front in the geographic zone affected by subduction of the Carnegie Ridge and is an optimal place to address the topic of adakites in arcs. Indeed, IVC volcanic rocks have characteristics that vary from calc-alkaline to adakitic.

We here present:

(1) the geology, mineralogy and composition of IVC products;

(2) the determination and quantification of the petrogenetic processes implied in IVC magma genesis,

(3) a discussion of the significance of the evolution of these processes over time.

2. Geological setting

The Iliniza volcanic complex (Hidalgo, 2001, 2002), is a large, almost circular (9 km NW–SE × 8 km NE–SW), edifice with twin peaks and two satellite domes (Fig. 1). The IVC is located in the Western Cordillera of Ecuador, built over a volcano-sedimentary basement composed of the Silante Unit and the Zumbagua Group, both of which are underlain by the Pallatanga Unit (Hughes, 1998; Hughes and Pilatasig, 2002). The Silante Unit is a Late Eocene to Oligocene volcano-sedimentary sequence of continental material including sandstone red beds, lacustrine deposits and andesitic breccias. The Middle to Late Miocene Zumbagua Group is made up of sandstones and volcanic breccias, also deposited in a continental environment. The Pallatanga Unit is composed of pillow lavas with compositional affinity to MORB. This unit is considered either as a fragment of oceanic floor (Goosens and Rose, 1973; Lebrat et al., 1987) or as an oceanic plateau (Cosma et al., 1998; Reynaud et al., 1999; Hughes and Pilatasig, 2002) accreted to the continent during the Late Cretaceous.

A set of N 40°E right-lateral strike-slip faults, the Iliniza Fault Zone (Fig. 1), cut the IVC and are part of the regional Pallatanga–Algeciras–Sibundoy fault system (Hall and Ramón, 1978; Soulas et al., 1991). The satellite domes of the IVC (Tishigcuchi and Pilongo) define a parallel alignment, suggesting the fault system controlled emplacement and growth of the edifices in the complex.

North Iliniza (5105 meters above sea level, m.a.s.l.) constitutes the older part, the base, of the main volcanic edifice. It is formed by ancient Pleistocene andesitic and dacitic lava flows and abundant altered sub-glacial breccias. The typical phenocryst assemblage comprises plagioclase + orthopyroxene + Fe-oxides + clinopyroxene.

South Iliniza (5245 m.a.s.l.), is a large stratocone, built at least several hundred thousands years after the North Iliniza, is made of andesitic and dacitic lava flows and thick pyroclastic flow deposits located in the outer flancs. This edifice suffered an explosive event, which formed a small caldera 1 km in diameter (Fig. 1). The *Jatuncama ignimbrite* deposits associated with this explosive event crop out on the lower slopes of the edifice and include dacitic blocks and pumices. A 25 cm "pumice and ash" flow deposit containing rhyolitic composition pumices overlies the ignimbrite only in the eastern side of the cone (*Santa Rosa* Pumice and Ash flow). A dome, with associated "block and ash" deposits and lava flows, subsequently filled this caldera and constitutes the pyramidal summit of the South Iliniza. The typical mineralogical assemblage of South Iliniza lavas and pyroclastic deposits includes plagioclase + Fe–Ti oxides ± orthopyroxene ± clinopyroxene ± amphibole ± apatite ± quartz. The older moraines, which cover the whole edifice, have their lower limits at 3400 m.a.s.l. They correspond to the Full Glacial Period (Clapperton, 1990) and therefore yield a minimum age of 30 Ka.

Two important satellite domes have been recognized in the complex (Fig. 1). The Pilongo Dome (3935 m.a.s.l.) is made of a microcrystalline dacitic lava including plagioclase + amphibole + Fe–Ti oxides + quartz ± orthopyroxene. The Tishigcuchi Dome (4185 m.a.s.l.) is composed of intersertale to microcrystalline silicic andesites (plagioclase + amphibole + orthopyroxene + clinopyroxene + Fe–Ti oxides ± quartz). No corresponding dome-collapse deposits have been found associated with these domes.

No absolute ages have been established for the edifices of the complex. Nevertheless, based on their erosional morphology and field relationships, the older seems to be North Iliniza, followed by the base of the South Iliniza, the Tishigcuchi Dome, the Pilongo Dome, and at last the newer part of the South Iliniza edifice, including the Jatuncama ignimbrite, the Santa Rosa pumice and ash flow, and the summit caldera filling deposits. If we make an analogy between the IVC and the dated volcanoes of the volcanic front, we can argue that the age of the older edifice, the North Iliniza, should be around 1 My and the base of South Iliniza would start its activity around 200 ky BP.

Based on field work as well as on geochemical data, four different units have been identified:

(1) the North Iliniza products,

(2) the South Iliniza and the Santa Rosa pumice and ash flow,

(3) the Pilongo Dome; and

(4) the Tishigcuchi Dome.

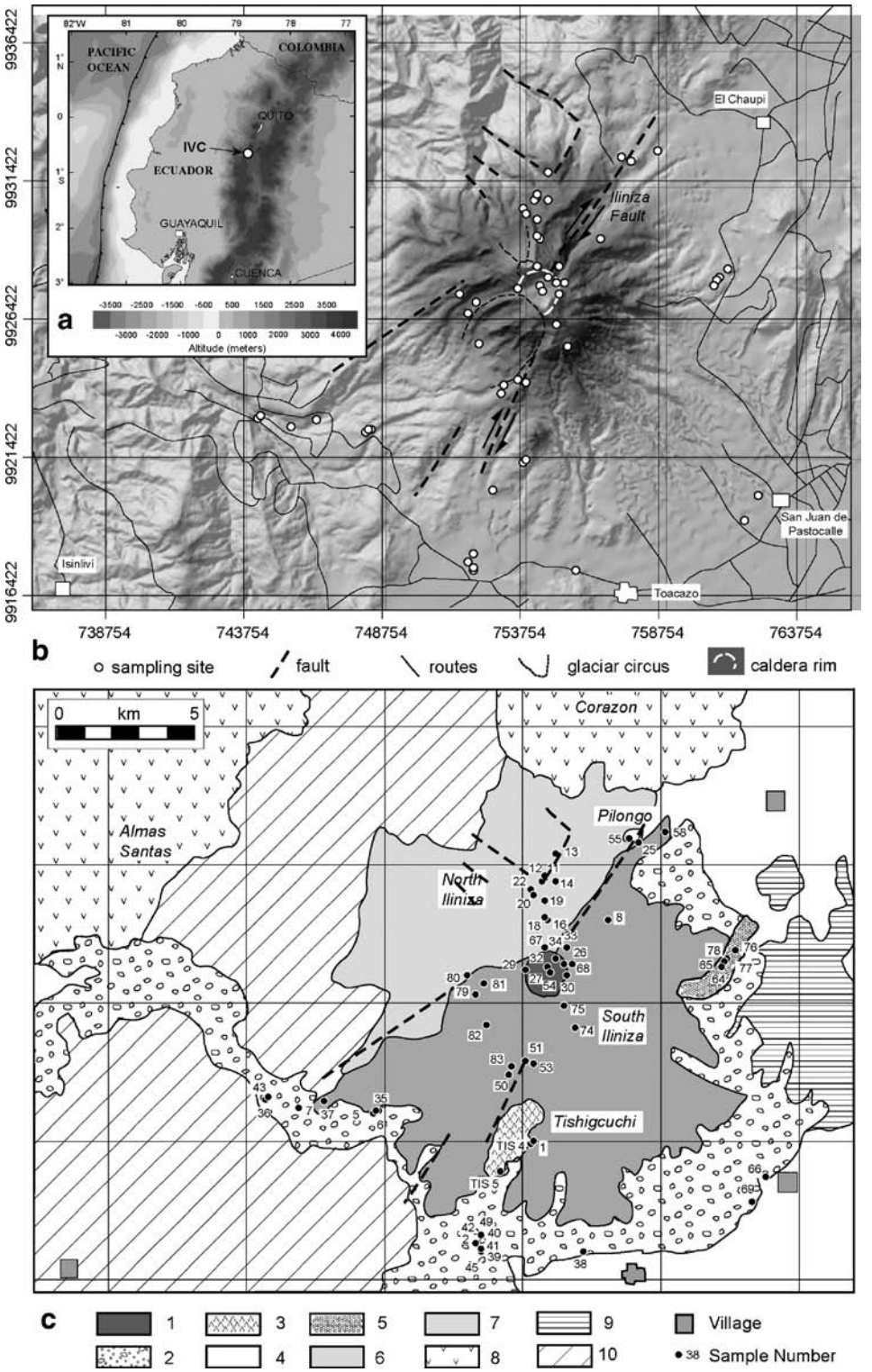


Fig. 1. (a) Location of the Iliniza Volcanic Complex in the Ecuadorian cordillera; (b) shaded DEM with the main morphostructural features of the volcanic complex; (c) simplified geological map of the Iliniza Volcanic Complex showing the sampling sites (UTM zone 17). 1 = South Iliniza Dome; 2 = Jatuncama Ignimbrite, deposits from South Iliniza; 3 = Tishigcuchi Dome; 4 = Pilongo Dome; 5 = Santa Rosa Pumice and Ash flow; 6 = South Iliniza ancient lavas; 7 = North Iliniza ancient lavas; 8 = Quaternary Volcanic Complexes (Almas Santas and Corazón); 9 = Pliocene Santa María Volcanic Complex; 10 = Silante and Zumbagua Eocene–Miocene Units.

Table 1
Major and trace elements compositions for amphibole, orthopyroxene, plagioclase and clinopyroxene from samples ILI 1A and ILI 50

	Tishigcuchi Dôme				South Iliniza											
Sample	ILI 1A	ILI 1A	ILI 1A	BCR	ILI 50	ILI 50	ILI 50	ILI 50	ILI 50	ILI 50	ILI 50	ILI 50	ILI 50	ILI 50	BCR	Limit of detection
Mineral	Amp	Amp	Amp	2σ	Opx	Pla	Pla	Pla	Pla	Pla	Cpx	Cpx	Cpx	Cpx	2σ	
number	28208	28209	28210	(s.d.)	1302	1304	1305	1306	1307	1308	1309	1310	1311	1312	(s.d.)	
(Weight %)																
SiO_2	43.59	43.35	43.06		53.43	58.27	57.04	58.19	55.98	57.32	50.94	51.29	51.27	51.95		
TiO_2	2.51	2.35	2.42		0.17	0.00	0.04	0.08	0.00	0.00	0.35	0.30	0.37	0.33		
Al_2O_3	11.56	11.30	10.90		2.76	26.56	27.21	26.34	27.88	27.15	3.63	2.60	2.05	3.24		
Fe_2O_3*	12.71	13.38	16.91		14.17	0.27	0.38	0.20	0.22	0.28	7.61	8.16	10.49	8.40		
FeO	11.44	12.04	15.22		12.75	0.25	0.34	0.18	0.20	0.26	6.85	7.35	9.44	7.56		
MnO	0.26	0.21	0.30		0.20	0.00	0.04	0.00	0.03	0.00	0.11	0.13	0.22	0.19		
MgO	15.28	15.08	12.94		29.11	0.03	0.01	0.02	0.01	0.04	16.95	16.74	16.68	16.22		
CaO	11.37	11.31	10.83		1.42	8.20	9.07	8.22	9.82	8.91	19.59	20.49	19.51	20.09		
Na_2O	2.23	2.43	1.98		0.05	6.82	6.23	6.83	5.96	6.40	0.41	0.42	0.19	0.40		
K_2O	0.43	0.43	0.32		0.00	0.35	0.39	0.36	0.30	0.35	0.00	0.01	0.02	0.02		
P_2O_5	0.00	0.00	0.02		0.04	0.00	0.04	0.00	0.05	0.01	0.10	0.00	0.06	0.00		
Cr_2O_3	0.04	0.02	0.04		0.44	0.00	0.00	0.02	0.03	0.00	0.70	0.31	0.10	0.34		
NiO	0.01	0.00	0.00		0.02	0.02	0.02	0.00	0.00	0.00	0.04	0.02	0.03	0.00		
Total	98.71	98.51	98.02		100.40	100.50	100.42	100.23	100.24	100.43	99.67	99.64	99.95	100.34		
(ppm)																
Rb	0.81	1.00	0.70	***5.52***	0.26	0.39	0.40	0.23	0.27	0.22	0.17	–		0.28	*19.52*	0.09
Ba	90	90	70	***1.27***	4.6	125	278	208	191	219	8.1	7.4	1.9	5.2	*95.88*	0.02
Th	0.033	0.045	0.044	***0.71***	0.059	–	–	–	–	–	0.030	0.020	–	0.030	*0.14*	0.01
Nb	2.9	3.1	3.5	***0.00***	0.09	–	–	–	–	–	0.09	–	–	–	*1.70*	0.04
La	3.1	3.4	4.4	***0.99***	0.12	2.1	4.3	4.9	4.6	3.6	0.8	0.5	0.4	0.4	*2.55*	0.02
Ce	12.6	15.1	18.3	***0.14***	0.36	3.4	5.8	6.4	7.0	5.5	2.4	2.5	2.4	2.5	*6.65*	0.02
Sr	256	229	105	***7.78***	3.0	864	827	801	961	776	27	20	20	24	*37.62*	0.04
Nd	15.4	18.1	21.8	***0.57***	0.22	0.86	1.4	1.6	1.6	1.3	2.5	3.7	3.1	3.0	*3.68*	0.12
Sm	5.0	5.7	7.0	***0.28***	0.09	0.07	0.15	0.14	0.09	0.16	0.9	1.3	1.4	1.3	*0.28*	0.10
Zr	27.3	31.9	42.2	***12.16***	2.0	–	0.08	–	0.09	–	6.7	10.4	9.0	7.8	*5.66*	0.05
Eu	1.48	1.63	1.77	***0.11***	0.025	0.41	0.74	0.56	0.59	0.60	0.34	0.48	0.44	0.39	*0.00*	0.02
Ti	16276	16705	14720	***129***	1058	74.5	91.8	59.6	67.8	88.4	1960	2880	2562	2587	*531*	1.96
Gd	4.9	5.8	7.5	***0.85***	0.09	0.12	0.22	0.16	0.14	0.15	1.0	1.4	1.5	1.2	*0.71*	0.05
Dy	4.0	4.6	6.5	***0.71***	0.21	0.031	0.039	0.021	–	–	1.2	1.7	1.6	1.2	*0.42*	0.03
Y	19.4	21.0	31.2	***1.98***	1.13	0.07	0.14	0.08	0.09	0.22	5.6	8.5	7.6	6.3	*2.26*	0.03
Er	1.85	1.96	3.0	***0.14***	0.16	–	–	0.017	–	–	0.6	0.8	0.7	0.7	*0.42*	0.25
Yb	1.46	1.6	2.6	***0.14***	0.19	–	0.013	–	–	0.017	0.45	0.8	0.6	0.5	*0.14*	0.02

3. Analytical techniques

Major and trace elements compositions were obtained for minerals and glasses from the different edifices of the IVC at the Laboratoire Magmas et Volcans of the University of Clermont-Ferrand. 236 major element compositions for mineral and glasses were obtained using an electron microprobe CAMECA-Camebax SX-100, operating at 15 kV accelerating voltage, and using a beam current of 15 nA for mineral analyses, and 8 nA and a 5 μm defocused beam for glass analyses. The estimated error for single analysis is of about 1% when the element concentration is higher than 10% and of 2–5% when it is lower than 10%. Trace element concentrations for 26 selected minerals were measured by Laser Ablation-ICP-MS technique. Laser ablation analyses were performed on mineral zones which major elements compositions were already constrained by electron microprobe analysis. Calcium was used as an internal standard (Table 1. Representative Analyses). The ICP-MS device used for the laser ablation is a VG Elemental Plasma Quad PQ 2+, with an argon flux of 1.15 l/min. The laser is a pulsed Nd:YAG operating at 266 nm, at a repetition rate of 6 Hz, with a spot diameter of approximately 60 μm and a pulse energy of about 2 mJ. The background was measured during 30 s before ablation, and analysis time was approximately 100 s. Data reduction was performed by the GLITTER software (www.es.mq.edu.au/GEMOC/). Reproducibility and accuracy of the analyses was constrained by systematic analysis of the BCR2-G (Columbia River Basalt) standard and are better than 15% for most elements, and often better than 5% for the REE (Table 1).

74 major and trace element whole-rock analyses (Table 2) of samples of lava flows, domes and pyroclastic deposits (both dense and vesiculated rocks), were carried out at the Université de Bretagne Occidentale. Chemical analyses were obtained on agate-ground powders by ICP-AES (Inductively coupled Plasma-Atomic Emission Spectroscopy), except for Rb (flame atomic emission). Relative standard deviation are 1% for SiO_2 and 2% for the other major elements except for low concentrations (<0.50%) for which absolute standard deviation is 0.01%. Analytical procedure is described in detail in Cotten et al. (1995).

4. Mineralogical data

IVC volcanic rocks from lava flows and domes present a porphyritic–aphanitic texture with an intersertal groundmass for the lavas and an intergranular microcrystalline groundmass for the domes.

Plagioclase phenocrysts (5–40% vol.) are typically euhedral with a composition ranging from andesine to labradorite ($An_{38–65}$). For Iliniza (North and South) and Tishigcuchi products, zoning is highly variable, normal ($An_{c52–r41}$; c=core, i=intermediate zone, r=rim), reversed ($An_{c40–r60}$) or oscillatory ($An_{c41–i67–r47}$). However, in the Pilongo Dome the plagioclase presents a normal zoning ($An_{c55–i45–r39}$) and rare reverse zoning ($An_{c42–r58}$). Some plagioclase crystals have destabilized reabsorbed cores and dusty reaction rims. In Iliniza products, plagioclase microlites are more sodic than the phenocrysts, ranging from andesine to oligoclase ($An_{29–45}$), whereas in Tishigcuchi microlites are frequently more calcic ($An_{50–60}$). Pilongo microlites have the same compositional range as the phenocrysts.

Clinopyroxene is present in Iliniza and Tishigcuchi lavas. There, it appears as euhedral to subhedral phenocrysts (0–15% vol.) of augite to magnesian augite (Mg# 85.6–70.9) (Morimoto et al., 1988). It generally has a normal zoning, but commonly, intermediate zones are slightly more magnesian than cores (i.e. reversed or recurrent zoning). No clinopyroxene has been observed in Pilongo Dome.

Orthopyroxene is present in both Iliniza and Tishigcuchi as euhedral and subhedral, phenocrysts (0–25% vol.) of normally zoned enstatite (Mg# 87.5–60.9). A particular feature of Tishigcuchi rocks is that hypersthene may coexist in close association with augite (i.e. in the same crystal, being the clinopyroxene an overgrowth on the orthopyroxene). In Pilongo and Santa Rosa rhyolites, orthopyroxene is only present as microlite in almost negligible amounts.

Brown amphibole (0–20% vol.) is euhedral and it usually has a destabilized oxidation rim. It mainly consists of tshermakite with subordinate magnesium-hastingsite and magnesium hornblende (Mg# 73–54) (Leake et al., 1997). Zoning is very weak and reversed in Iliniza whereas it is normal in Pilongo, Santa Rosa rhyolites and Tishigcuchi rocks. Representative mineral compositions are shown in Table 3.

It is important to note that orthopyroxene and clinopyroxene maximum contents diminish from North Iliniza (the older edifice) to Pilongo Dome and Santa Rosa rhyolites (the younger units) as the amphibole content is incremented in the opposite direction, being the richer amphibole bearing rocks the Pilongo rhyodacites and the Santa Rosa rhyolites. The absence of pyroxene crystals and the abundance of amphibole is a typical characteristic of high SiO_2 adakites (Martin et al., 2005).

Table 2
Geochemical major and trace element data for the Iliniza Volcanic Complex

	North Iliniza	North Iliniza	North Iliniza	North Iliniza	North Iliniza	North Iliniza	North Iliniza	North Iliniza	South Iliniza	South Iliniza	South Iliniza	South Iliniza	South Iliniza	South Iliniza	South Iliniza	South Iliniza	South Iliniza	South Iliniza	South Iliniza
Sample	ILI 58B	ILI 58A	ILI 16B	ILI 14A	ILI 11	ILI 22A	ILI 18	ILI 19A	ILI 45	ILI 50	ILI 81	ILI 51	ILI 82	ILI 79B	ILI 79A	ILI 5	ILI 7A	ILI 2B	ILI 36C
Weight %																			
SiO_2	55.30	55.50	61.40	62.50	62.60	62.70	64.00	64.20	56.80	61.00	61.80	62.00	62.00	62.10	62.40	62.80	63.30	63.40	63.50
TiO_2	0.83	0.90	0.58	0.57	0.58	0.58	0.58	0.56	0.70	0.66	0.61	0.66	0.57	0.63	0.65	0.57	0.54	0.59	0.54
Al_2O_3	16.90	17.75	15.90	16.30	16.00	16.00	16.40	16.25	17.40	16.20	16.20	16.00	16.20	16.40	16.30	16.00	16.00	15.85	16.00
Fe_2O_3*	8.80	8.40	6.42	6.07	5.99	5.91	5.54	5.34	8.05	6.82	6.62	6.72	6.10	6.36	6.55	5.80	5.50	5.97	5.55
MnO	0.13	0.12	0.11	0.09	0.09	0.09	0.09	0.08	0.11	0.10	0.09	0.10	0.09	0.09	0.10	0.09	0.09	0.09	0.08
MgO	5.55	4.13	3.55	2.82	2.80	2.78	2.28	2.17	4.13	3.68	3.54	3.41	3.70	2.91	3.00	2.68	2.75	2.69	2.58
CaO	7.50	7.50	6.00	5.45	5.45	5.45	5.37	5.22	7.40	5.75	5.80	5.70	5.70	5.75	5.80	5.24	4.95	5.40	5.15
Na_2O	3.58	3.94	3.68	3.85	4.06	3.91	4.15	3.92	3.62	3.87	3.98	3.84	3.97	3.84	3.81	4.03	4.22	4.04	4.10
K_2O	0.82	1.01	1.34	1.47	1.49	1.49	1.48	1.41	0.88	1.15	1.07	1.20	1.29	1.33	1.26	1.51	1.35	1.24	1.32
P_2O_5	0.17	0.22	0.15	0.15	0.15	0.15	0.16	0.15	0.15	0.14	0.14	0.14	0.14	0.14	0.14	0.15	0.14	0.15	0.15
LOI	0.63	0.46	0.82	0.26	0.55	0.48	0.04	0.27	0.46	0.30	0.28	0.19	−0.03	0.13	0.17	0.88	0.85	0.17	0.60
Total	100.21	99.93	99.95	99.53	99.76	99.54	100.09	99.57	99.70	99.67	100.13	99.96	99.73	99.68	100.18	99.75	99.69	99.59	99.57
FeO*/MgO	1.43	1.83	1.63	1.94	1.93	1.91	2.19	2.21	1.75	1.67	1.68	1.77	1.48	1.97	1.97	1.95	1.80	2.00	1.94
Mg #	55.53	49.33	52.26	47.91	48.07	48.22	44.90	44.59	50.39	51.65	51.43	50.12	54.57	47.53	47.56	47.78	49.75	47.15	47.93
(ppm)																			
Sc	23.5	20.0	17.3	15.6	13.2	12.8	11.0	11.0	20.0	14.8	13.0	13.7	14.5	13.2	14.0	12.6	12.0	13.3	11.3
V	212	214	148	138	134	134	145	118	182	148	136	144	145	138	140	126	110	125	116
Cr	202	34	83	44	60	59	22	22	70	140	115	117	140	62	67	51	60	52	59
Co	30	24	19	17	17	17	15	14	22	19	20	19	18	17	18	15	14	17	15
Ni	67	26	21	16	17	19	10	9	22	41	41	33	43	22	23	14	20	19	22
Rb	14	18	29	30	31	31	31	31	16	22	19	23	26	30	27	31	26	25	28
Sr	454	617	410	410	420	425	465	447	464	427	422	429	424	400	397	426	417	419	415
Y	18.6	17.0	14.2	11.0	12.5	11.8	10.5	10.0	13.6	10.6	9.6	11.4	11.6	12.2	12.5	12.4	11.2	10.9	10.8
Zr	90	103	107	106	115	112	76	103	69	76	77	90	82	98	96	110	92	94	90
Nb	3.5	5.0	3.3	2.9	3.7	4.0	3.6	3.3	2.4	3.3	3.1	3.5	3.0	4.0	4.1	3.2	3.4	3.6	3.7
Ba	392	450	590	632	610	630	640	645	344	495	460	520	546	542	540	612	530	560	565
La	12.0	12.5	11.0	10.8	12.0	11.6	12.0	11.4	7.7	8.8	9.1	10.3	10.4	10.8	11.2	11.0	10.3	9.7	10.5
Ce	24.0	27.0	22.5	22.5	24.5	24.0	24.0	23.0	16.0	18.5	20.0	21.0	21.5	23.5	26.0	24.5	21.5	20.0	20.8
Nd	16.0	16.0	12.6	11.2	13.0	13.0	12.8	12.3	10.8	10.6	11.0	12.5	10.8	12.5	13.0	12.5	11.5	11.0	12.5
Sm	4.00	3.70	2.90	2.35	2.80	3.00	2.80	2.75	2.60	2.60	2.70	2.75	2.85	3.10	2.85	2.70	2.60	2.50	2.60
Eu	1.14	1.09	0.82	0.81	0.83	0.82	0.83	0.80	0.87	0.85	0.81	0.86	0.79	0.86	0.88	0.81	0.79	0.77	0.78
Gd	3.70	3.60	2.95	2.45	2.90	2.70	2.65	2.55	2.95	2.45	2.30	2.80	2.45	2.75	2.85	2.80	2.60	2.60	2.60
Dy	3.25	2.95	2.40	2.00	2.20	2.15	1.95	1.85	2.45	1.95	1.80	2.05	2.05	2.30	2.30	2.15	1.95	1.90	1.95
Er	1.80	1.65	1.30	1.10	1.20	1.15	1.00	1.00	1.30	1.00	0.90	1.05	1.00	1.10	1.20	1.10	1.00	0.95	0.95
Yb	1.64	1.58	1.25	1.02	1.04	1.02	0.86	0.85	1.17	0.93	0.83	0.93	1.06	1.01	1.05	1.01	0.95	0.88	0.95
Th	1.50	2.30	2.30	2.50	2.80	2.65	2.40	2.75	1.35	2.00	1.85	2.25	2.20	2.25	2.35	2.60	2.40	2.10	2.35

All data are normalized on a LOI free basis. Total iron is expressed as Fe_2O_3. NI=North Iliniza, SI=South Iliniza. BE-N is an international standard from GIT-IWG (groupe international de travail-international working group), analysed as an unknown in the same set than Iliniza analyses; recommended values were published by Govindaraju and Roelandts (1993).

Table 2 (*continued*)

	South Iliniza	South Iliniza	South Iliniza	South Iliniza	South Iliniza	South Iliniza	South Iliniza	South Iliniza	South Iliniza	Iliniza Rhyolite	Pilongo Dome	Pilongo Dome	Tishigc. Dome	Tishigc. Dome	Tishigc. Dome	Tishigc. Dome	Pasochoa Volcano	Standard BE-N	Limit of detection
Sample	ILI 77A2	ILI 4A	ILI 35A	ILI 41	LI 32B2	TIS 1	ILI 43	ILI 4B	ILI 29A	ILI 64	ILI 55B	ILI 25	ILI 37A	ILI 1A	TIS 4B	ILI 1B	PAS 5		
Weight %																			
SiO_2	63.60	64.00	64.25	64.30	64.35	64.60	64.80	65.00	66.50	70.00	67.50	68.10	59.80	61.90	62.00	62.30	55	38.23	
TiO_2	0.57	0.55	0.55	0.57	0.52	0.52	0.56	0.53	0.48	0.32	0.34	0.36	0.60	0.60	0.60	0.58	0.74	2.62	
Al_2O_3	16.00	16.00	16.40	16.00	15.80	16.10	15.90	16.25	15.40	14.85	16.65	15.90	15.65	15.25	15.52	15.38	16.3	10.03	
Fe_2O_3*	5.79	5.37	5.45	5.60	5.03	5.27	5.53	5.20	4.40	2.78	3.47	3.54	6.60	6.17	6.17	6.00	9.01	12.80	
MnO	0.08	0.08	0.08	0.08	0.08	0.08	0.08	0.08	0.06	0.05	0.06	0.06	0.10	0.10	0.09	0.09	0.14	0.20	
MgO	2.54	2.18	2.45	2.51	2.18	2.17	2.35	2.14	1.79	0.68	0.94	0.99	4.45	3.68	3.54	3.39	6.14	13.18	
CaO	5.25	4.82	5.10	5.02	4.95	4.80	4.98	4.85	4.30	3.06	3.95	3.77	6.35	5.92	5.76	5.83	7.75	13.93	
Na_2O	4.06	4.17	4.15	4.02	4.10	4.25	4.07	4.29	4.24	4.54	4.52	4.40	3.85	3.88	3.95	3.93	3.4	3.25	
K_2O	1.25	1.58	1.35	1.33	1.37	1.36	1.35	1.38	1.52	1.42	1.40	1.45	1.65	1.59	1.60	1.57	0.65	1.39	
P_2O_5	0.14	0.15	0.14	0.15	0.15	0.13	0.14	0.14	0.13	0.12	0.14	0.14	0.20	0.18	0.17	0.18	0.15	1.04	
LOI	0.53	0.60	0.48	0.25	1.28	−0.08	0.04	−0.06	1.37	1.96	0.81	1.06	0.55	0.44	0.38	0.39	0.34		
Total	99.81	99.50	100.40	99.83	99.81	99.20	99.80	99.80	100.19	99.78	99.78	99.77	99.80	99.71	99.78	99.64	99.62		
FeO*/MgO	2.05	2.22	2.00	2.01	2.08	2.19	2.12	2.19	2.21	3.68	3.32	3.22	1.33	1.51	1.57	1.59	1.32		
Mg #	46.48	44.56	47.09	47.02	46.18	44.91	45.69	44.90	44.61	32.63	34.91	35.64	57.17	54.15	53.18	52.80	57.43		
(ppm)																			(ppm)
Sc	11.0	10.7	12.0	12.0	9.8	10.2	10.4	10.3	7.8	2.3	4.2	4.5	15.6	16.0	14.0	15.0	24.5	22	0.1
V	124	113	115	118	104	107	109	107	88	33	54	55	152	143	136	139	204	230	1
Cr	57	30	43	51	36	31	44	30	35	6	4	5	130	106	101	102	210	354	1
Co	16	15	15	14	13	13	12	14	11	4	5	6	25	20	19	20	35	59.5	1
Ni	15	12	15	20	15	11	15	13	12	6	3	3	78	35	30	33	87	267	1
Rb	25	27	27	26	29	28	26	28	32	30	28	30	33	32	32	32	11	47	0.5
Sr	412	423	408	425	420	405	425	414	405	455	470	448	620	550	548	546	425	1349	0.5
Y	10.2	10.7	11.0	10.2	11.0	10.0	10.4	10.2	8.1	5.5	7.2	7.2	11.9	12.0	11.2	11.2	14.0	29.3	0.3
Zr	84	98	97	91	85	96	87	94	51	76	72	60	88	100	97	102	80	265	3
Nb	3.5	3.3	3.3	3.6	3.5	3.6	3.6	3.3	3.8	4.6	3.5	3.6	4.1	3.9	4.0	4.1	2.7	104	0.5
Ba	530	570	535	575	600	560	570	570	655	705	600	760	665	650	620	690	347	1012	1
La	10.9	10.0	10.2	10.8	12.5	10.2	11.5	11.0	12.0	16.1	11.8	12.5	18.0	15.0	15.6	14.6	8.5	83	0.5
Ce	22.0	21.5	22.0	22.0	24.5	22.5	22.0	22.5	23.0	33.0	24.5	25.0	35.0	28.0	31.5	30.0	16.5	150	1.5
Nd	12.1	11.5	12.0	12.1	13.7	11.5	12.8	11.2	12.7	17.0	13.5	13.8	19.0	16.0	16.0	15.0	11.5	67	0.6
Sm	2.85	2.55	2.75	2.75	2.80	2.55	2.60	2.70	2.60	3.00	2.90	2.55	3.80	3.25	3.35	3.00	2.9	12.25	0.6
Eu	0.80	0.77	0.76	0.79	0.82	0.73	0.82	0.77	0.74	0.91	0.79	0.76	1.03	0.96	0.91	0.91	0.92	3.65	0.15
Gd	2.55	2.45	2.40	2.40	2.70	2.20	2.60	2.50	2.30	2.90	2.10	2.15	3.05	2.85	2.60	3.00	2.9	9.5	1
Dy	1.90	1.90	1.95	1.95	1.95	1.70	1.85	2.00	1.55	1.20	1.40	1.45	2.15	2.10	1.95	1.90	2.5	6.35	0.3
Er	1.00	0.95	1.05	1.00	0.95	1.00	1.00	1.00	0.80	0.50	0.70	0.60	1.10	1.15	1.00	1.10	1.3	2.8	1
Yb	0.84	0.87	0.93	0.94	0.92	0.85	0.86	0.89	0.65	0.37	0.56	0.55	0.96	0.96	0.92	0.90	1.25	1.84	0.15
Th	2.30	2.30	2.20	2.35	2.40	2.20	2.25	2.40	2.70	2.50	2.00	1.95	3.40	3.50	3.40	3.10	1.1	10.6	0.3

Table 3
Major elements compositions from representative mineral phases from the IVC rocks

Clinopyroxene

	North Iliniza							South Iliniza				Tishigcuchi							
Sample	SIL 16B	SIL 16B	SIL 16B	SIL 16B	SIL 16B	SIL 16B	SIL 16B	SIL 50	SIL 50	SIL 50	SIL 50	SIL 1a	SIL 1a	SIL 1a(e)	SIL 1a(e)	SIL 1a(e)	SIL 1a(e)	SIL 37	SIL 37
Grain	CPX-1	CPX-1	CPX-1	CPX-1	CPX-2	CPX-2	CPX-2	CPX-1	CPX-1	CPX-2	CPX-2	CPX-1	CPX-2	CPX-1	CPX-1	OPX-1	CPX-2	CPX-1	CPX-1
zone	CORE	INT	INT	RIM	CORE	INT	RIM	CORE	RIM	CORE	RIM	RIM		CORE	RIM	CORE	INT	INT	RIM
SiO_2	52.18	49.90	51.05	49.20	51.34	50.59	49.49	51.95	51.27	51.29	50.96	51.41	50.76	49.84	51.07	54.35	51.76	51.35	51.26
TiO_2	0.43	0.89	0.41	1.00	0.41	0.47	0.71	0.33	0.37	0.30	0.38	0.34	0.45	0.43	0.43	0.16	0.24	0.37	0.58
Al_2O_3	3.52	3.85	3.34	4.14	4.47	4.16	4.65	3.24	2.05	2.60	2.24	2.34	2.92	4.30	3.30	2.69	2.45	3.49	5.03
MnO	0.15	0.17	0.19	0.26	0.19	0.19	0.25	0.19	0.22	0.13	0.45	0.24	0.19	0.42	0.24	0.28	0.09	0.20	0.29
MgO	16.72	14.73	17.10	14.25	15.93	16.43	14.19	16.22	16.68	16.74	16.18	15.22	16.07	13.83	16.35	30.60	17.03	16.16	14.59
CaO	20.96	19.60	20.10	19.71	20.90	20.45	19.86	20.09	19.51	20.49	19.59	21.21	21.12	21.30	20.25	2.05	20.82	20.68	19.78
Na_2O	0.36	0.36	0.34	0.31	0.38	0.34	0.31	0.40	0.19	0.42	0.29	0.41	0.33	0.59	0.40	0.10	0.38	0.00	0.77
K_2O	0.00	0.01	0.00	0.01	0.00	0.00	0.02	0.02	0.02	0.01	0.00	0.00	0.00	0.00	0.02	0.00	0.00	0.00	0.06
P_2O_5	0.10	0.00	0.05	0.03	0.00	0.00	0.04	0.00	0.06	0.00	0.03	0.00	0.08	0.03	0.01	0.02	0.05	0.05	0.04
Cr_2O_3	0.21	0.20	0.42	0.00	0.14	0.11	0.00	0.34	0.10	0.31	0.06	0.05	0.17	0.02	0.12	0.71	0.23	0.12	0.00
NiO	0.00	0.00	0.00	0.05	0.00	0.00	0.00	0.00	0.03	0.02	0.01	0.02	0.00	0.00	0.05	0.02	0.01	0.04	0.00
FeO	6.44	9.30	6.48	10.45	6.71	7.02	10.28	7.56	9.44	7.35	9.49	8.90	7.62	9.04	7.31	10.13	6.40	7.39	8.73
Total	101.07	99.02	99.47	99.41	100.46	99.77	99.80	100.34	99.95	99.64	99.69	100.13	99.70	99.80	99.55	101.09	99.46	99.85	101.15
En	42.30	41.30	47.10	40.10	43.50	45.30	39.70	44.50	46.30	46.30	45.10	42.30	44.60	38.60	45.20	79.90	47.00	44.50	39.90
Fs	14.30	14.90	10.30	16.90	10.60	11.20	16.50	11.90	15.10	11.60	15.60	14.30	12.20	14.90	11.70	15.30	10.00	11.70	13.80
Wo	40.90	35.80	37.50	36.40	36.70	37.20	35.80	36.60	38.40	39.40	38.40	40.90	40.60	39.20	37.70	2.20	39.80	37.70	33.60

Orthopyroxene

	North Iliniza		South Iliniza									Tishigcuchi									
Sample	SIL 16B	SIL 16B	SIL 50	SIL 50	SIL 50	SIL 50	SIL 50	SIL 4B	SIL 4B	SIL 4B	SIL 4B	SIL 1a	SIL 1a	SIL 1a	SIL 1a	SIL 37	SIL 37	SIL 37	SIL 37	SIL 37	SIL 37
Grain	OPX-4	OPX-4	OPX-1	OPX-2	OPX-2	OPX-4	OPX-4	OPX-1	OPX-1	OPX-3	OPX-3	OPX-9	OPX-9	OPX-10	OPX-2	OPX-1	OPX-1	OPX-4	OPX-4	OPX-4	OPX-3
zone	CORE	RIM	RIM	INT	RIM	CORE	RIM	CORE	RIM	CORE	RIM	CORE	RIM	microlite	microlite	CORE	RIM	CORE	INT	RIM	microlite
SiO_2	52.95	53.75	54.01	53.43	55.10	54.29	51.74	51.82	53.54	55.04	53.04	53.98	53.07	53.87	55.05	53.22	53.28	54.05	54.31	53.83	53.51
TiO_2	0.09	0.27	0.17	0.17	0.25	0.05	0.34	0.07	0.11	0.02	0.11	0.17	0.13	0.33	0.25	0.08	0.20	0.10	0.12	0.20	0.20
Al_2O_3	0.84	0.94	2.49	2.76	3.04	2.67	3.35	1.28	1.36	2.48	1.24	2.71	1.28	2.89	3.74	1.78	2.35	1.87	2.44	3.11	3.00
MnO	0.70	0.66	0.35	0.20	0.22	0.20	0.07	0.72	0.70	0.14	0.70	0.20	0.54	0.61	0.55	0.17	0.30	0.26	0.19	0.20	0.18
MgO	22.33	23.16	28.84	29.11	26.17	29.78	25.07	22.74	25.04	31.44	24.31	29.93	25.69	21.65	20.07	34.38	29.13	29.36	31.41	30.47	28.56
CaO	0.96	1.18	1.39	1.42	1.62	1.51	1.92	0.46	0.86	1.15	0.73	1.35	1.06	1.96	3.36	1.36	1.36	1.63	1.52	1.69	1.79
Na_2O	0.00	0.05	0.02	0.05	0.12	0.04	0.01	0.04	0.03	0.06	0.00	0.13	0.08	0.38	0.80	0.10	0.03	0.06	0.00	0.07	0.05
K_2O	0.03	0.00	0.02	0.00	0.02	0.00	0.00	0.00	0.01	0.00	0.03	0.00	0.01	0.39	0.39	0.01	0.02	0.01	0.00	0.00	0.02
P_2O_5	0.00	0.00	0.06	0.04	0.06	0.03	0.04	0.01	0.02	0.02	0.00	0.03	0.02	0.21	1.25	0.00	0.02	0.01	0.00	0.04	0.00
Cr_2O_3	0.02	0.04	0.36	0.44	0.00	0.34	0.02	0.02	0.00	0.74	0.02	0.31	0.00	0.00	0.00	0.49	0.10	0.00	0.46	0.61	0.23
NiO	0.01	0.00	0.02	0.02	0.02	0.11	0.02	0.00	0.00	0.09	0.02	0.00	0.01	0.02	0.01	0.09	0.02	0.02	0.04	0.09	0.02
FeO	22.09	21.82	13.27	12.75	16.17	11.90	17.74	22.17	19.12	9.83	19.56	11.91	17.96	18.22	17.71	8.79	12.90	13.48	10.21	10.71	12.56
Total	100.00	101.84	101.00	100.40	102.78	100.91	100.31	99.32	100.77	101.00	99.76	100.71	99.86	100.52	103.18	100.47	99.69	100.84	100.72	101.02	100.11
En	62.00	63.00	76.20	77.30	68.60	78.30	68.20	63.70	68.00	81.80	66.90	78.80	70.20	58.80	52.90	90.10	77.90	77.80	82.20	79.80	76.00
Fs	35.50	34.40	20.20	19.30	24.10	17.90	27.20	36.00	30.20	14.50	31.30	17.90	28.40	28.70	27.00	13.20	19.80	20.40	15.30	16.00	19.00
Wo	1.20	1.70	1.00	1.10	0.10	1.10	1.60	0.60	1.00	0.20	0.60	1.30	1.80	1.40	3.80	2.10	1.70	2.90	1.60	1.30	1.20

Plagioclase

	North Iliniza						South Iliniza															
Sample	SIL 16B	SIL 16B	SIL 16B	SIL 16B	SIL 16B	SIL 16B	SIL 50	SIL 50	SIL 50	SIL 50	SIL 50	SIL 50	SIL 50	SIL 50	SIL 4B	SIL 4B	SIL 4B	SIL 4B	SIL 4B	SIL 4B	SIL 4B	SIL 4B
Grain	PLG-1	PLG-1	PLG-2	PLG-2	PLG-3	PLG-4	PLG-1	PLG-1	PLG-1	PLG-1	PLG-1	PLG-2	PLG-2	PLG-2	PLG-1	PLG-1	PLG-2	PLG-2	PLG-3	PLG-4	PLG-5	
zone	CORE	RIM	CORE	INT	CORE	microlite	ORE	INT I	INT II	INT III	RIM	CORE	INT	RIM	CORE	RIM	CORE	INT I	RIM	microlite	microlite	microlite
SiO_2	57.19	55.08	58.21	56.05	56.29	57.26	58.27	56.24	57.54	57.04	58.58	55.98	58.19	53.83	57.78	54.77	55.19	55.13	57.74	57.59	57.97	62.37
TiO_2	0.00	0.04	0.00	0.00	0.01	0.09	0.00	0.00	0.02	0.04	0.00	0.00	0.08	0.03	0.00	0.09	0.05	0.00	0.02	0.01	0.01	0.01
Al_2O_3	26.45	28.03	26.25	27.57	27.14	26.79	26.56	28.14	26.74	27.21	26.30	27.88	26.34	29.64	26.59	28.25	28.10	27.91	26.32	26.33	25.90	23.19
MnO	0.00	0.03	0.00	0.00	0.05	0.02	0.00	0.00	0.09	0.04	0.00	0.03	0.00	0.00	0.03	0.00	0.02	0.00	0.00	0.04	0.00	0.01
MgO	0.04	0.03	0.02	0.00	0.03	0.05	0.03	0.03	0.01	0.01	0.01	0.01	0.02	0.05	0.00	0.03	0.00	0.04	0.01	0.00	0.06	0.00
CaO	8.82	10.50	8.42	9.78	9.60	9.15	8.20	9.65	8.64	9.07	7.71	9.82	8.22	11.71	8.62	10.74	10.78	10.16	8.45	8.55	7.92	5.29
Na_2O	6.40	5.60	6.62	5.82	5.93	6.19	6.82	5.97	6.83	6.23	6.66	5.96	6.83	4.80	6.74	5.54	5.63	5.82	6.92	6.55	6.84	7.61
K_2O	0.43	0.35	0.31	0.27	0.27	0.37	0.35	0.27	0.31	0.39	0.50	0.30	0.36	0.22	0.20	0.28	0.26	0.15	0.25	0.66	0.81	1.20
P_2O_5	0.02	0.00	0.00	0.00	0.00	0.04	0.00	0.00	0.01	0.04	0.00	0.05	0.00	0.05	0.02	0.02	0.00	0.02	0.03	0.02	0.00	0.07
Cr_2O_3	0.00	0.00	0.00	0.00	0.00	0.02	0.00	0.01	0.03	0.00	0.04	0.03	0.02	0.00	0.01	0.00	0.00	0.00	0.00	0.05	0.00	0.00
NiO	0.01	0.00	0.01	0.00	0.00	0.00	0.02	0.01	0.01	0.02	0.02	0.00	0.00	0.01	0.00	0.00	0.01	0.00	0.00	0.01	0.00	0.01
FeO	0.28	0.34	0.16	0.16	0.36	0.63	0.25	0.17	0.26	0.34	0.34	0.20	0.18	0.80	0.25	0.34	0.28	0.23	0.26	0.43	0.37	0.27
Total	99.65	99.99	99.99	99.63	99.68	100.60	100.50	100.49	100.49	100.42	100.16	100.24	100.23	101.13	100.22	100.04	100.31	99.46	100.01	100.24	99.89	100.03
An	43.60	51.30	41.90	48.90	47.90	45.40	40.50	47.90	41.80	45.00	39.20	48.30	40.50	58.10	42.40	52.40	52.10	50.20	41.10	41.70	38.50	26.90
Ab	53.90	46.60	56.30	49.60	50.50	52.40	57.40	50.50	56.40	52.70	57.80	50.00	57.40	40.60	56.50	46.00	46.40	49.00	57.40	54.50	56.80	65.90
Or	2.50	2.00	1.80	1.60	1.60	2.20	2.10	1.60	1.80	2.30	3.10	1.70	2.10	1.30	1.20	1.60	1.50	0.90	1.50	3.90	4.70	7.20

	Tishigcuchi											Pilongo									
Sample	SIL 1a	SIL 1a	SIL 1a	SIL 1a	SIL 1a	SIL 1a	SIL 1a	SIL 1a	SIL 37	SIL 37	SIL 37	SIL 25	SIL 25	SIL 25	SIL 25	SIL 25	SIL 25	SIL 25	SIL 25	SIL 25	SIL 25
Grain	PLG-3	PLG-3	PLG-3	PLG-3	PLG-5	PLG-5	PLG-1	PLG-2	PLG-1	PLG-1	PLG-1	PLG-5	PLG-5	PLG-5	PLG-5	PLG-7	PLG-7	PLG-7	PLG-7	PLG-2	PLG-4
zone	CORE	INT I	INT III	RIM	core	RIM	microlite	microlite	CORE	INT	RIM	CORE	INT II	INT II	RIM	CORE	INT I	INT II	RIM	microlite	microlite
SiO_2	55.30	53.71	57.87	54.67	50.15	53.78	53.10	59.27	58.99	59.41	58.79	57.47	56.43	57.79	58.71	57.59	59.09	58.22	57.95	58.11	58.51
TiO_2	0.00	0.02	0.00	0.02	0.01	0.01	0.01	0.11	0.03	0.03	0.05	0.00	0.00	0.01	0.00	0.00	0.02	0.01	0.00	0.00	0.00
Al_2O_3	28.46	29.29	26.31	27.62	31.17	28.79	28.49	24.12	25.20	24.96	25.26	26.67	27.56	27.29	26.54	26.46	25.25	27.10	26.76	26.54	26.05
MnO	0.00	0.00	0.03	0.02	0.03	0.04	0.00	0.00	0.01	0.00	0.00	0.00	0.00	0.00	0.00	0.02	0.00	0.00	0.00	0.04	0.05
MgO	0.00	0.00	0.01	0.04	0.03	0.05	0.08	0.04	0.03	0.00	0.02	0.03	0.01	0.00	0.03	0.03	0.00	0.01	0.01	0.01	0.02
CaO	10.52	11.76	8.09	10.53	14.52	11.85	11.77	8.54	7.34	7.00	7.30	8.50	9.35	8.94	7.81	8.29	7.18	8.70	8.41	8.24	7.58
Na_2O	5.68	4.89	7.12	5.67	3.48	4.83	4.88	5.50	7.49	7.66	7.11	6.68	6.38	6.47	6.89	6.68	7.19	6.50	6.44	6.72	7.07
K_2O	0.16	0.16	0.27	0.22	0.10	0.21	0.18	0.83	0.56	0.50	0.61	0.33	0.18	0.19	0.38	0.17	0.26	0.16	0.32	0.39	0.43
P_2O_5	0.00	0.02	0.05	0.04	0.00	0.11	0.02	0.10	0.00	0.05	0.00	0.06	0.00	0.05	0.00	0.00	0.03	0.03	0.01	0.05	0.03
Cr_2O_3	0.00	0.05	0.00	0.03	0.00	0.00	0.01	0.00	0.01	0.01	0.00	0.00	0.02	0.03	0.02	0.00	0.02	0.04	0.00	0.00	0.01
NiO	0.01	0.00	0.01	0.01	0.00	0.03	0.00	0.01	0.00	0.00	0.00	0.00	0.01	0.06	0.01	0.00	0.02	0.00	0.00	0.02	0.04
FeO	0.17	0.26	0.22	0.43	0.51	0.57	0.72	0.85	0.10	0.10	0.24	0.25	0.14	0.21	0.19	0.12	0.13	0.15	0.28	0.19	0.25
Total	100.29	100.16	99.98	99.29	100.01	100.28	99.24	99.36	99.75	99.72	99.39	99.99	100.07	101.03	100.56	99.35	99.18	100.92	100.18	100.31	100.05
An	51.60	57.90	39.30	51.50	70.60	58.30	58.00	45.20	35.30	33.90	36.20	41.90	45.80	44.20	39.00	41.70	36.30	43.60	42.50	40.90	37.60
Ab	47.50	41.10	59.10	47.20	28.90	40.50	41.00	49.60	61.40	63.20	60.20	56.20	53.20	54.60	58.70	57.30	62.10	55.50	55.50	56.80	59.80
Or	0.90	1.00	1.60	1.30	0.60	1.20	1.10	5.20	3.20	2.90	3.60	1.90	1.00	1.10	2.20	1.00	1.60	0.90	1.90	2.30	2.60

(continued on next page)

Table 3 (*continued*)

Glass

	North Iliniza	Tishigcuchi			Pilongo			
Sample	SIL 16B	SIL 1a	SIL 1a	SIL 1a	SIL 25	SIL 25	SIL 25	SIL 25
Grain	Glass-2	Glass	Glass	Glass	Glass-1	Glass-2	Glass-4	Glass-5
zone	matrix	matrix	matrix	matrix	matrix	matrix	matrix	matrix
SiO_2	75.15	77.71	77.78	76.29	81.91	82.17	81.79	82.32
TiO_2	0.36	0.62	0.54	0.37	0.07	0.05	0.12	0.11
Al_2O_3	13.93	11.14	11.14	11.91	10.95	11.20	11.30	10.53
MnO	0.05	0.01	0.07	0.00	0.00	0.07	0.02	0.00
MgO	0.02	0.07	0.03	0.05	0.13	0.08	0.07	0.05
CaO	1.35	0.47	0.45	0.92	1.61	1.76	1.82	1.50
Na_2O	3.89	2.04	2.16	2.92	4.35	4.50	4.39	4.30
K_2O	3.50	4.22	3.88	3.48	0.51	0.47	0.50	0.52
P_2O_5	0.26	0.05	0.06	0.02	0.11	0.00	0.20	0.06
Cr_2O_3	0.00	0.00	0.00	0.00	0.00	0.03	0.09	0.00
NiO	0.00	0.01	0.00	0.01	0.02	0.00	0.00	0.01
FeO	0.97	1.30	1.23	1.06	0.19	0.09	0.19	0.38
Total	99.46	97.63	97.35	97.03	99.83	100.43	100.48	99.78

Apatite

	Pilongo	
Sample	SIL 25	SIL 25
Grain	APT-1	APT-1
zone	CORE	RIM
SiO_2	0.08	0.09
TiO_2	0.00	0.00
Al_2O_3	0.00	0.00
MnO	0.13	0.46
MgO	0.18	0.38
CaO	54.97	54.50
Na_2O	0.06	0.06
K_2O	0.01	0.01
P_2O_5	43.60	43.65
Cr_2O_3	0.00	0.00
NiO	0.01	0.00
FeO	0.18	1.10
Total	99.20	100.25

Amphibole

	South Iliniza								Tishigcuchi									
Sample	SIL 4B	SIL 4B	SIL 4B	SIL 4B	SIL 4B	SIL 4B	SIL 4B	SIL 4B	SIL 1a	SIL 1a	SIL 1a	SIL 1a	SIL 1a	SIL 1a	SIL 1a	SIL 1a	SIL 1a	SIL 37
Grain	AMP-1	AMP-1	AMP-2	AMP-2	AMP-3	AMP-3	AMP-4	AMP-4	AMP-1	AMP-1	AMP-2	AMP-2	AMP-3	AMP-3	AMP-3	AMP-4	AMP-4	AMP-1
zone	CORE	RIM	CORE	RIM	CORE	REACT. RIM	CORE	RIM	CORE	RIM	CORE	RIM	CORE	INT	RIM	CORE	RIM	CORE
	f-t-ts	f-mg-hbda	f-t-ts	f-mg-hbda	f-ts	f-ts-hbda	f-t-ts	ti-mg-has	f-mg-hbda	f-ts-hbda	f-t-ts	f-ts-hbda	f-t-ts	f-t-ts	f-ts-hbda	ti-mg-has	f-t-ts	mg-hbda
SiO_2	42.55	46.30	44.30	46.70	41.90	44.02	42.30	41.42	46.39	44.13	41.86	43.97	42.44	42.37	44.89	42.49	43.83	44.03
TiO_2	2.65	1.17	2.39	1.49	2.14	2.05	2.56	2.60	1.35	2.05	2.49	2.09	2.41	2.50	1.64	2.52	2.40	1.61
Al_2O_3	10.78	7.85	9.97	8.36	12.72	10.53	11.88	11.90	8.13	9.78	12.10	9.90	11.33	12.07	9.50	11.48	10.25	7.18
MnO	0.20	0.35	0.26	0.29	0.07	0.24	0.14	0.13	0.27	0.18	0.13	0.16	0.19	0.14	0.27	0.13	0.20	0.30
MgO	13.82	15.85	13.90	15.19	14.41	14.76	13.99	13.77	15.23	14.76	14.42	15.03	14.72	15.44	14.95	14.89	14.67	14.72
CaO	10.77	10.29	11.17	10.75	11.39	10.98	10.77	11.20	10.84	11.12	11.28	11.31	11.29	11.24	11.00	11.32	11.05	15.53
Na_2O	2.36	3.14	2.00	2.05	2.41	2.17	2.50	2.63	1.82	2.25	2.28	2.13	2.37	2.37	2.06	2.39	2.13	0.81
K_2O	0.30	0.20	0.31	0.26	0.29	0.24	0.33	0.34	0.24	0.30	0.43	0.37	0.48	0.40	0.34	0.43	0.42	0.74
P_2O_5	0.04	0.00	0.01	0.10	0.06	0.06	0.02	0.02	0.00	0.04	0.00	0.17	0.00	0.04	0.06	0.06	0.05	0.00
Cr_2O_3	0.02	0.00	0.03	0.04	0.05	0.00	0.00	0.00	0.04	0.04	0.00	0.06	0.00	0.01	0.01	0.05	0.00	0.04
NiO	0.00	0.02	0.03	0.00	0.00	0.02	0.01	0.02	0.01	0.00	0.00	0.00	0.00	0.02	0.00	0.05	0.00	0.00
FeO	13.64	12.73	13.78	13.32	12.18	12.68	13.11	12.97	13.66	13.08	11.83	12.45	12.36	11.70	12.92	11.08	12.38	14.29
Total	97.11	97.90	98.13	98.54	97.61	97.74	97.61	97.02	97.97	97.71	96.82	97.62	97.58	98.30	97.64	96.89	97.36	99.26

Amphibole

	Tishigcuchi				Pilongo					
Sample	SIL 37	SIL 37	SIL 37	SIL 37	SIL 25	SIL 25	SIL 25	SIL 25	SIL 25	SIL 25
Grain	AMP-1	AMP-2	AMP-2	AMP-2	AMP-1	AMP-1	AMP-3	AMP-3	AMP-4	AMP-4
zone	RIM	CORE	INT	RIM	CORE	REACTION RIM	CORE	RIM	CORE	RIM
	act-hbda	f-ts	f-ts	f-ts	mg-has	f-ts	f-ts	f-ts	f-ts	f-ts
SiO_2	51.56	42.31	42.32	42.28	41.50	41.43	42.57	40.83	41.74	42.28
TiO_2	1.16	1.87	1.83	1.79	1.98	1.22	1.75	1.33	0.90	1.07
Al_2O_3	6.23	12.95	13.06	13.02	13.19	13.06	13.39	13.60	13.18	13.10
MnO	0.36	0.15	0.12	0.14	0.09	0.22	0.15	0.24	0.35	0.35
MgO	15.59	15.34	14.96	15.10	12.48	11.65	13.00	10.95	11.33	11.42
CaO	13.72	11.05	11.19	10.78	10.76	10.02	10.34	10.24	9.81	10.12
Na_2O	1.42	2.51	2.45	2.62	3.01	2.06	2.30	2.43	2.95	2.38
K_2O	0.12	0.59	0.56	0.53	0.36	0.44	0.34	0.37	0.27	0.34
P_2O_5	0.04	0.00	0.02	0.00	0.08	0.01	0.12	0.00	0.00	0.03
Cr_2O_3	0.00	0.06	0.03	0.05	0.08	0.00	0.03	0.00	0.00	0.00
NiO	0.00	0.01	0.00	0.02	0.00	0.04	0.00	0.00	0.01	0.02
FeO	9.49	11.46	11.12	11.45	15.02	16.67	13.54	16.57	16.83	16.78
Total	99.68	98.29	97.65	97.78	98.56	96.81	97.53	96.56	97.36	97.89

Oxides

	North Iliniza			Tishigcuchi	Pilongo		
Sample	SIL 16B	SIL 16B	SIL 16B	SIL 1a	SIL 25	SIL 25	SIL 25
Grain	ILM-1	Ti-MAG-1	Ti-MAG-1	Ti-MAG	Ti-MAG-1	Ti-MAG-2	ILM-1
zone	INT	INT	INT		CORE	INT	INT
SiO_2	0.01	0.05	0.05	0.85	0.09	0.02	0.41
TiO_2	33.15	9.01	8.44	12.56	3.65	12.27	50.35
Al_2O_3	0.26	1.23	2.37	1.78	3.80	2.48	0.05
MnO	0.09	0.24	0.21	0.33	0.42	0.62	1.13
MgO	1.47	0.75	1.56	0.95	0.64	0.76	1.90
CaO	0.01	0.03	0.01	1.21	0.00	0.01	0.06
Na_2O	0.02	0.02	0.00	0.03	0.00	0.01	0.00
K_2O	0.00	0.02	0.00	0.10	0.00	0.00	0.00
P_2O_5	0.03	0.01	0.00	0.94	0.00	0.05	0.00
Cr_2O_3	0.03	0.06	0.17	0.01	0.08	0.03	0.00
NiO	0.03	0.02	0.00	0.05	0.00	0.02	0.03
FeO	60.61	83.03	81.55	74.45	84.94	79.45	45.72
Total	95.73	94.47	94.36	93.25	93.62	95.72	99.66

f-t-ts	ferri-titanian-tschermakite
f-mg-hbda	ferri-magnesio-hornblende
f-ts	ferri-tschermakite
f-ts-hbda	ferri-tschermakitic hornblende
ti-mg-has	titanian-magnesio-hastingsite
mg-hbda	magnesio-hornblende
act-hbda	actinolitic hornblende
mg-has	magnesio-hastingsite

f-t-ts ferri-titanian-tschermakite; *f-mg-hbda* ferri-magnesio-hornblende; *f-ts* ferri-tschermakite; *f-ts-hbda* ferri-tschermakitic hornblende; *ti-mg-has* titanian-magnesio-hastingsite; *mg-hbda* magnesio-hornblende; *act-hbda* actinolitic hornblende; *mg-has* magnesio-hastingsite.

5. Distribution coefficients

In order to perform a geochemical modelling best adapted to our lavas, we tried to calculate mineral/liquid partition coefficients (Kds) for our rocks. Calculations were done on phenocryst-poor (10–15% in vol.) samples (ILI 1A and ILI 50). Laser Ablation-ICP-MS has been used to measure the trace element contents of phenocrysts. Knowing (1) the percentage of each mineral phase in the sample (modal composition) and (2) the whole rock trace element composition; it has been possible to calculate the theoretical liquid compositions in equilibrium with phenocrysts. These data allowed the Kd calculation. Results are shown in Table 4. Clinopyroxene and amphibole calculated Kds are similar to those measured by Klein et al. (2000) and also to the average Kds compiled by Martin (1987), Rollinson (1993) and Green (1994) for equivalent liquid compositions. Kds for plagioclase also perfectly fall in the range of experimental values by Fujimaki et al. (1984) and of those measured by Luhr and Carmichael (1980) and Bacon and Druitt (1988) in andesitic and dacitic liquids.

6. Whole rock data

In IVC rocks, SiO_2 concentrations range from 55 to 71 wt.%. In the K_2O vs. SiO_2 classification diagram (Peccerillo and Taylor, 1976) their compositions range between the basic andesite and medium-K rhyolite fields, but the majority of analysed samples are andesites and dacites (Fig. 2). Mg# varies between 0.32 and 0.58. Harker diagrams (Fig. 3) show marked negative correlations between SiO_2 and Fe_2O_3, MgO, CaO and TiO_2 contents. A general negative correlation can also be noted for Al_2O_3 and P_2O_5, whereas Na_2O and K_2O concentrations correlate positively with SiO_2 content. The North Iliniza rocks are more basic (55.30 to 64.20 wt.% SiO_2) and present a slight enrichment in incompatible elements (Rb, Ba, Th) with respect to South Iliniza rocks (Fig. 4). Tishigcuchi products display a more restricted range of composition (60 to 63% SiO_2), and are richer in MgO, K_2O and P_2O_5 than South Iliniza rocks. Pilongo rocks consist of very homogeneous rhyodacites, around 69% SiO_2, which for major elements fit into the general trend of the South Iliniza.

For South Iliniza products Zr, Sc, V, Cr and Ni are negatively correlated with SiO_2 whereas Rb, La and Ba show a positive correlation (Fig. 4). Also, for some trace elements, Pilongo products fit into the South Iliniza trend. This is not true for Tishigcuchi products, which for instance, have greater Rb, Sr, Nb, La and Th concentrations than all of the other lavas from the IVC (Fig. 4).

It must be emphasized that both Y and Yb (HREE) show a general negative correlation with SiO_2. Y and Yb concentrations are generally low (<14 ppm and <1.1 ppm respectively), except for the more basic North Iliniza rocks, thus resulting in strongly fractionated REE patterns. These low concentrations are classically

Table 4
Distribution coefficients calculated from laser ablation and data for clinopyroxene, amphibole and plagioclase (cursive)

Distribution coefficients						
Element	Clinopyroxene	Amphibole	Plagioclase	Magnetite	Apatite	Zircon
La	*0.062*	*0.252*	*0.458*	0.22	25	2
Ce	*0.136*	*0.58*	*0.311*	0.26	35	2.64
Nd	*0.295*	*1.259*	*0.13*	0.3	58	2.2
Sm	*0.478*	*2.073*	*0.048*	0.35	64	3.14
Eu	*0.516*	*2.002*	*0.725*	0.26	30	3.14
Gd	*0.529*	*2.488*	*0.066*	0.28	64	12
Dy	*0.746*	*2.877*	*0.016*	0.28	58	101.5
Er	*0.715*	*2.294*	*0.017*	0.22	40	135
Yb	*0.646*	*2.291*	*0.014*	0.18	22	527
Rb	*0.009*	*0.026*	*0.014*	0.18	16	345
Ba	*0.012*	*0.133*	*0.425*	0.00001	2	0.00001
Nb	*0.021*	*0.854*	*0.009*	0.00001	0.00001	140
Sr	*0.062*	*0.414*	*2.303*	0.00001	0.00001	0.00001
Zr	*0.112*	*0.345*	*0.001*	0.00001	0.01	3800
Y	*0.673*	*2.312*	*0.012*	0.00001	0.00001	140
V	1.1	6	0.01	8.6	0.00001	0.00001
Cr	8.4	8.4	0.01	8	0.00001	0.00001
Co	2.2	6.5	0.03	0.00001	0.00001	25
Ni	4.8	12	0.1	9.5	0.2	0.00001

Apatite, Magnetite and Zircon distribution coefficients from Martin (1987) used in the fractional crystallization model are also shown.

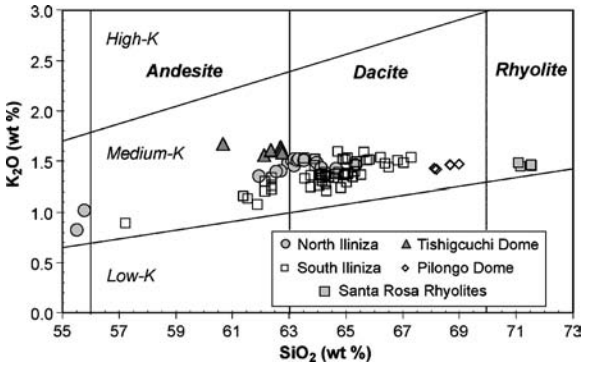


Fig. 2. K_2O vs. SiO_2 classification diagram for orogenic magmas (Peccerillo and Taylor, 1976) for the Iliniza Volcanic Complex series. Data are recalculated to 100% on an anhydrous basis.

considered as typical of high-SiO_2 adakites. Furthermore, Pilongo rhyodacites (ILI 25, 55A, 55B and 55C; Table 1) and the Santa Rosa rhyolites (ILI 64, 65, 77A1 and 78; Table 1) display strongly marked high-SiO_2 adakites characteristics: Yb = 0.35–0.61 ppm; Y = 5.4–7.8 ppm, La/Yb = 20.49–43.71 and Sr/Y = 58.21–84.26; and also high Na_2O (4.43–4.74 wt.%), K_2O/Na_2O (0.33–0.31), Al_2O_3 (14.85–16.65 wt.%) and Sr (453–470 ppm) concentrations (Drummond and Defant, 1990; Martin et al., 2005).

7. Petrogenesis

7.1. North Iliniza

North Iliniza rocks display geochemical characteristics very similar to those of the South Iliniza products. Consequently, both generally define a single evolution trend. However, when compared some small differences can be pointed out: (1) some samples of North Iliniza are more basic (55% SiO_2); (2) for the same SiO_2 content, North Iliniza rocks are richer in some incompatible elements such as K, Rb, Ba and Th. Classically, it is considered that incompatible element enrichment in arc lavas is due to fluid metasomatism (Tatsumi, 1986; Tatsumi, 1989), these elements are coming from the subducted slab whose dehydration creates an uprising fluid flux that transfers incompatible elements towards the overlying mantle wedge peridotite. At IVC, as in other Ecuadorian volcanoes, a temporal change from calc-alkaline magmatism to adakites is observed (Samaniego et al., 2002, 2005). These authors consider that this change consists in a change of the nature of the metasomatic agent, which is first dehydration fluid and then turns into slab melt. They also propose that this change in magmatism could result of the arrival of the Carnegie ridge under the volcanic arc. In this context, the North Iliniza magmas that display calc-alkaline affinities, can be considered as generated by melting of a fluid metasomatized mantle peridotite, without significant slab melt input.

7.2. South Iliniza

In order to constrain South Iliniza petrogenesis, quantitative modelling has been performed. Shallow processes (i.e. crustal) are modelled first, then, in a second stage, deep processes are considered. Mineralogical and geochemical evidence, such as the zoned phenocrysts, the well-correlated trends between incompatible elements, and the strong decrease in compatible elements with differentiation (Fig. 3), indicates that fractional crystallization played an important role in magma evolution. Accordingly, this process has been tentatively quantified: the tested model explores the possibility to generate the more evolved magmas from the less differentiated ones by a simple fractional crystallization process. In Harker diagrams (Fig. 3) major elements define a differentiation trend, but they also slightly scatter around it. Accordingly, the best trend fitting data has been calculated. Major element modelling tries to reproduce this trend that has been theoretically defined with parent and daughter magmas with 60 and 68 SiO_2 % respectively. Then, composition of the cumulative assemblage is calculated using a simple mass-balance algorithm (Stormer and Nicholls, 1978). Trace element variations have been modelled using the classical Rayleigh (1896) equation and the composition of samples ILI 50 and ILI 29A (Table 2) as parent and daughter magmas respectively. Major element compositions for the fractioning minerals are an average of those obtained using the electron microprobe (Table 5). Partition coefficients are those calculated from phenocryst/liquid pairs (Table 4); Kd for magnetite, apatite and zircon were taken from Martin (1987) compilation. Results of calculation are shown in Table 5 for major element and as multi-element primitive mantle normalized diagram for trace elements (Fig. 5). The observed trend for South Iliniza products could result from about 37% of fractional crystallization of a cumulate made up of 58% amphibole, 38% plagioclase, 2.2% clinopyroxene, 1% magnetite, 0.1% apatite and 0,05% zircon. It is important to note that the computed modal composition of the cumulate is very similar to that of the crustal xenoliths found in Colombia (Weber et al., 2002). When this modal composition is introduced in trace element modelling (Fig. 5) calculated liquid composition perfectly fits sample ILI 29A composition. As both major and trace element

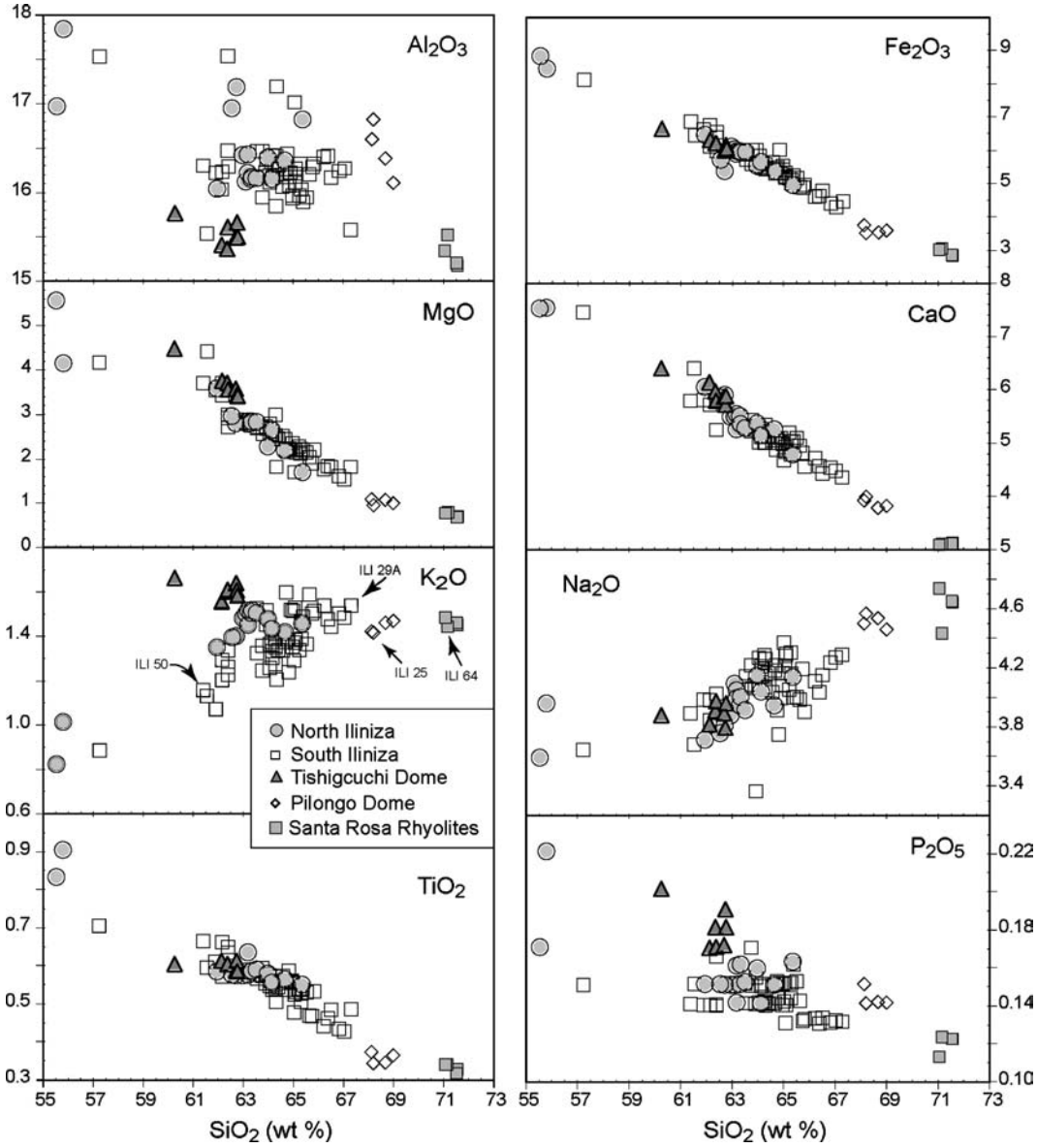


Fig. 3. Harker's diagrams for the Iliniza Volcanic Complex rocks. Oxides values are recalculated to 100% on an anhydrous basis.

modelling converge towards a single coherent solution, it will be considered that fractional crystallization of an assemblage of amphibole, plagioclase and subordinate mineral phases in a crustal reservoir is a mechanism that realistically accounts for the last stages of the South Iliniza magma genesis.

These calculations allow to explain the differentiation trend by fractional crystallization, but of course the problem of the parental magma genesis remains. As the Ecuadorian volcanic arc is obviously related to subduction, and taking into account the geochemical characteristics of the South Iliniza rocks (calc-alkaline with little adakitic imprint), four possible petrogenetic mechanisms can be envisaged:

(1) Melting of a mantle wedge peridotite, previously metasomatized by hydrous fluids liberated by subducted slab dehydration. Nevertheless this option is not developed due to the relatively high SiO_2 content of the parental magma (>60% SiO_2) and its corresponding low Mg# (<52), which could not be in equilibrium with mantle wedge olivine;

(2) Melting of the subducted oceanic crust, either oceanic crust of the Nazca plate or the Carnegie Ridge. Several different basaltic compositions are thus

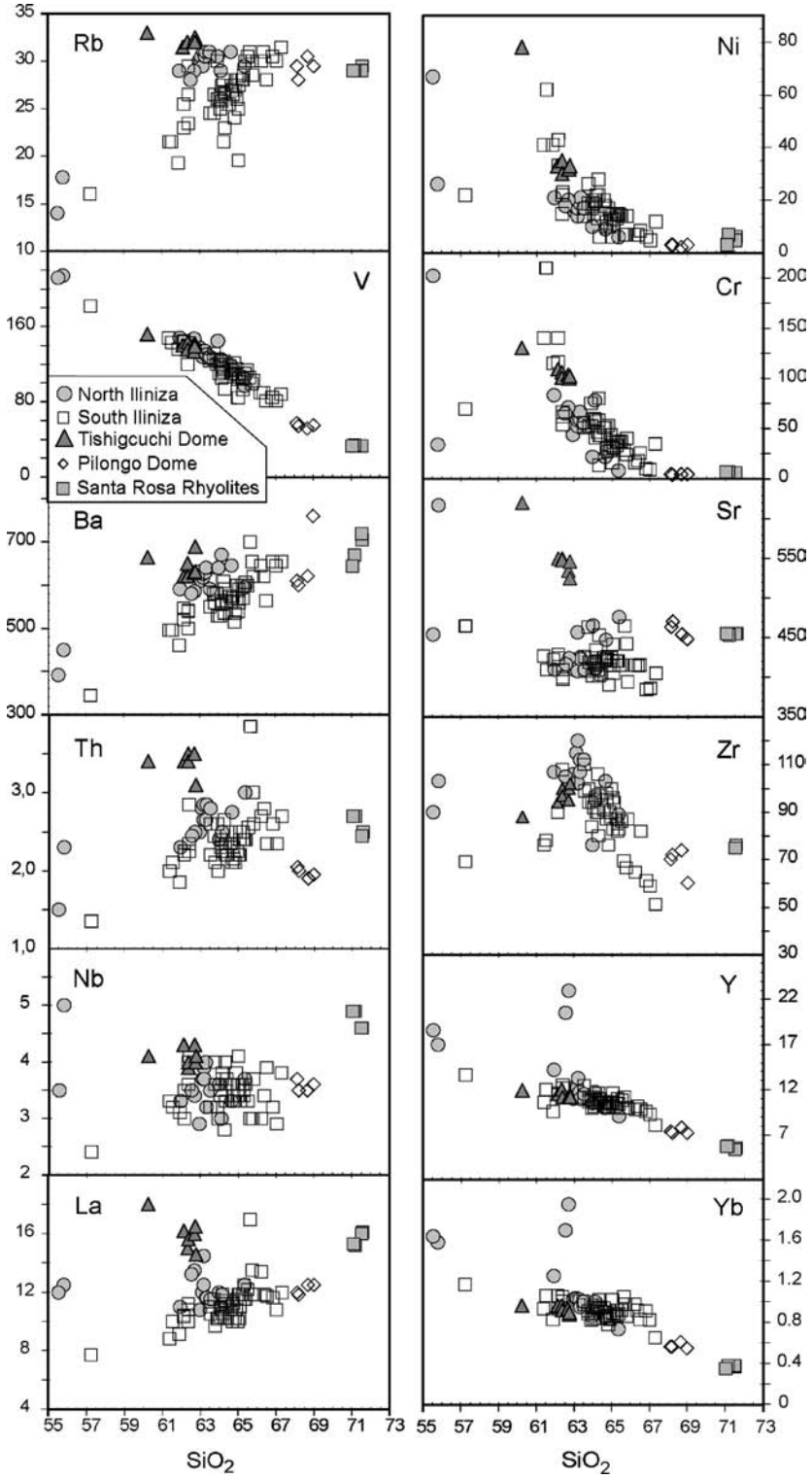


Fig. 4. Plots of selected trace elements concentrations (ppm) against SiO_2 (wt.%).

Table 5
Theorethical composition of the parental and daughter magmas for the Iliniza series

	Parental magma	Daughter magma	cpx	opx	pl1	pl2	am	Ti-mt	apt	Cumulate	Final liquid
SiO_2	60.00	68.00	50.82	51.81	57.55	53.81	42.14	0.102	0.09	***46.18***	***68.12***
TiO_2	0.65	0.49	0.49	0.14	0.02	0.02	1.44	18.50	–	***0.95***	***0.47***
Al_2O_3	17.06	15.69	3.42	2.38	26.69	28.29	13.57	1.67	–	***19.16***	***15.83***
Fe_2O_3	7.15	4.32	8.74	14.28	0.27	0.54	17.77	78.47	1.22	***11.78***	***4.43***
MgO	3.54	1.17	16.07	30.06	0.02	0.03	1.95	1.14	0.38	***7.47***	***1.23***
CaO	6.60	4.11	20.11	1.29	8.58	11.18	10.31	0.02	54.30	***10.65***	***4.22***
Na_2O	3.90	4.60	0.34	0.04	6.55	5.20	2.48	0.01	0.05	***3.47***	***4.15***
K_2O	1.09	1.67	0.01	–	0.032	0.33	0.34	0.003	0.01	***0.33***	***1.54***
% cumulate			***2.2***	–	–	***38.26***	***58.32***	***1.08***	***0.09***		
(1−F)%										***37***	
r^2										***0.11***	

Mineral compositions and results for the mass balance calculations. cpx=clinopyroxene, opx=orthopyroxene, pl1=andesine plagioclase, pl2=labradorite plagioclase, am=tschermakite, Ti-mt=titano-magnetite, apt=apatite, $(1-F)$=crystallization rate. Final liquids calculated composition is shown for comparison with the daughter magma.

considered as potential sources: two N-MORB compositions (Hofmann, 1988; Sun and Mcdonough, 1989) for the Nazca crust, and an E-MORB composition (Sun and Mcdonough, 1989) or a basaltic composition from Galapagos hotspot (Verma and Schilling, 1982) for the Carnegie Ridge (Table 2);

(3) Melting of underplated basalts. For this source, a basaltic composition (EAC) from accreted terranes of Western Ecuador (Arculus et al., 1999) is considered.

(4) Crustal contamination or AFC processes might also be envisaged for the genesis of these magmas. Nevertheless $^{87}Sr/^{86}Sr$ and $^{143}Nd/^{144}Nd$ isotopic compositions for the whole volcanic arc show that crustal contamination or crust assimilation did not play a significant role in the genesis of the Ecuadorian magmas (Bourdon et al., 2002b; Samaniego et al., 2005). These authors agree that crustal contamination might reach a maximum value of 10% in volume for the Eastern Cordillera volcanoes and that it is almost negligible for the volcanoes of the volcanic front. For this reason this hypothesis will not be further considered in this study.

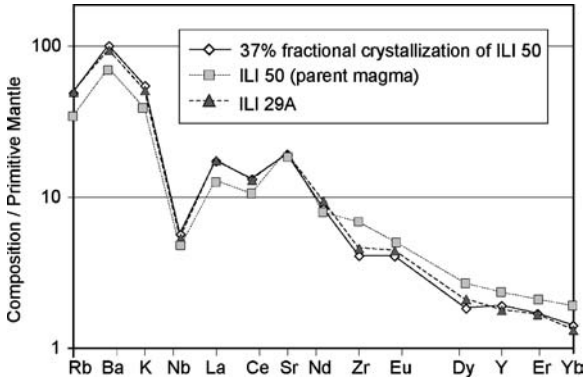


Fig. 5. Theoretical spidergram obtained by 37% of fractional crystallization from a magma with ILI 50 composition to obtain the most evolved lava of Iliniza Series (ILI 29A). Normalization to the primitive mantle of Sun and Mcdonough (1989).

In order to test items 2 and 3, modelling will proceed in two steps, first mass balance calculation based on major element behaviour, and subsequently trace element modelling based on the residue composition and degree of melting calculated with major elements. Compositions of sources and of residual mineral phases are respectively given in Tables 6 and 7. Calculations performed on basalts from the slab and the accreted eclogite give a reasonable but not excellent fit between the data and model ($r^2<1$) (Table 8). In all cases the degree of melting is of about 36%. It must be noted that the melting residue is always eclogitic in composition, which is perfectly consistent with P–T conditions at the estimated slab depth (100–120 km; Guillier et al., 2001) and with the continental crust thickness (~50 km; Prévot et al., 1996).

However, when applied to trace element the computed models for melting of slab basalts or accreted eclogite give discordant results, especially when the degree of melting (F) is considered; calculated F is always greater than 50% and even reaches 70% for the AEC sample, which is obviously unrealistic. In addition these calculations not only disagree with results obtained using major element data, but also they are obviously unrealistic when compared to F values obtained during basalt melting experiments (Sen and Dunn, 1994; Rapp and Watson, 1995; Zamora, 2000). Consequently, it appears that no one of these potential

processes can satisfactorily account for the genesis of the less differentiated South Iliniza magmas.

Nevertheless, as many minerals show complex, reversed or oscillatory zoning, and as some samples clearly present two different kinds of matrix, an origin by magma mixing for the more basic magmas has been tested. Taking into account the already mentioned adakitic imprint in South Iliniza products, a model of mixing, similar to the one proposed by Kilian et al. (1995) for Chimborazo products, has been tested. This model consists in a mixing between calc-alkaline and pristine adakitic magmas of the Quaternary Ecuadorian arc. In our case the magmas with a clear calc-alkaline affinity are those from the North Iliniza edifice and those from the neighbouring Pasochoa volcano (located 40 km NE of the IVC, in the Inter-Andean Valley). The selected sample to test our hypothesis is the high Mg-andesite PAS 5 (55.4% SiO_2, 6.2% MgO; Table 2), which is the most primitive lava found in the northern Ecuadorian volcanic arc. The chosen pristine adakitic composition is a rhyodacite from Pilongo Dome (ILI 25), whose origin by slab melting will be discussed below.

Mixing calculation (Fig. 6) (Fourcade and Allègre, 1981) results in a very good adjustment between theoretical and real magmas (correlation coefficient of $R^2=0.9892$) for the mixing between 36% of pristine adakitic and 64% of calc-alkaline magmas. Consequently, a possible way to account for South Iliniza parental magma composition could be mixing between melts from the mantle wedge and the subducted slab. These magmas were generated more or less contemporaneously and probably mixed in a mantle conduit during their transfer to the crust, at the base of the arc crust or in a crustal magma chamber, before eruption. The proposed mixing process is in good agreement with the mixing evidences observed in the South Iliniza rocks, such as reverse and oscillatory zoning and the coexistence of two kinds of matrix in the same sample.

7.3. Santa Rosa Rhyolites (South Iliniza)

Rhyolitic products belonging to the Santa Rosa pumice and ash flow, follow for major elements, the general differentiation trend shown by the South Iliniza. However, when a fractional crystallization is modelled the calculated degree of crystallization is extremely high and consequently appears as highly unrealistic even when computation implies a hypothetical more felsic parental magma. This can be seen in the K_2O vs. SiO_2 Harker diagram (Fig. 3), and is also confirmed by a Th/La vs. Rb diagram (Fig. 7), where the South Iliniza rocks show a subhorizontal trend while the rhyolites (together with Pilongo dacites) lie out of it. If the rhyolites were product of higher degrees of fractional crystallization of the same source, they should be placed in the continuity of the subhorizontal trend defined by the South Iliniza rocks.

In addition, these rocks are very similar in composition to Quimsacocha's rhyolitic adakites (Beate et al., 2001). Their high Sr/Y (78.1–78.3) and La/Yb (40.0–43.5) ratios, due to their important depletions in HREE (Yb = 0.35–0.38 ppm) and Y (5.4–5.8 ppm), are obvious evidences of their high SiO_2 adakitic affinity

Table 6
Source compositions considered for the modelling of partial melting processes

	Oceanic basalts				Accreted crust
	N-MORB	N-MORBs	E-MORBs	GSC	EAC
Reference	(1)	(2)	(3)	(4)	(5)
SiO_2	50.2	50.2	50.2	50.4	49.8
TiO_2	1.6	1.2	1.2	1.7	1.5
Al_2O_3	15.2	15.2	15.2	14.8	15.1
Fe_2O_3	11.5	11.5	11.5	11.3	12.5
MnO					0.2
MgO	7.5	7.5	7.5	7.2	7.6
CaO	11.3	11.3	11.3	11.6	10.7
Na_2O	2.7	2.7	2.7	2.6	2.3
K_2O		0.1	0.2	0.2	0.1
P_2O_5		0.1	0.1	0.2	0.2
Sc	41.4			42.1	75
V				330.9	602.2
Cr				191.8	172.6
Co	47.1			40.9	
Ni	149.5				58.7
Rb	1.3	0.6	5	4.2	0.6
Sr	113.2	90	155	117.5	88
Y	35.8	28	22		35.8
Zr	104.2	74	73		90.6
Nb		2.3	8.3		8.5
K		668.4	1670.4	1930.7	666.7
Ba	13.9	6.3	57	46.4	90.6
La	3.9	2.5	6.3	5.7	6.4
Ce	12	7.5	15	15.5	15.5
Nd	11.2	7.3	9	12.6	10.8
Sm	3.8	2.6	2.6	4.2	3.4
Eu	1.3	1	0.9	1.4	1.1
Gd	5.1	3.7	3		3.9
Dy	6.3	4.6	3.6		5.4
Er	4.1	3	2.3		3.4
Yb	3.9	3.1	2.4	3.9	3.5
Th	0.2	0.1	0.6		0.5

(1) N-MORB (Hofmann, 1988); (2) and (3) N-MORB and E-MORB (Sun and Mcdonough, 1989), major elements taken from Hofmann (1988); (4) basalt from the Galápagos Spreading Center (GSC, Verma and Schilling, 1982); (5) eclogotized basalt (Arculus et al., 1999).

Table 7
Residual mineral phases compositions

Reference	Mantle wedge partial melting					Basalt partial melting			
	Mantle xenoliths				Rapp et al., 1999	Experimental data			
	Kepezhinskas et al., 1995					Sen and Dunn, 1994			
	ol	cpx	opx	grt 1	grt 2	hbl	cpx	grt	rt
SiO_2	40.28	50.64	54.29	37.95	41.48	43.88	48.33	39.34	0.00
TiO_2	0.00	0.27	0.05	1.16	0.51	1.53	1.17	0.87	99.40
Al_2O_3	0.05	6.40	1.88	21.32	21.37	12.69	10.04	21.84	0.00
Fe_2O_3	11.67	5.41	6.82	26.99	18.02	17.59	11.01	22.06	0.56
MnO	0.13	0.06	0.10	0.97	0.36	0.35	0.00	0.45	0.00
MgO	48.68	17.40	35.89	3.05	17.03	11.35	9.98	9.23	0.00
CaO	0.34	19.49	1.46	11.22	2.50	11.82	18.14	8.43	0.10
Na_2O	0.02	0.72	0.17	0.03	0.51	1.85	1.94	0.00	0.00
K_2O	0.00	0.14	0.01	0.01	0.01	0.71	0.00	0.00	0.00

ol = olivine; cpx = clinopyroxene; opx = orthopyroxene; grt = garnet; hbl = hornblende; rt = rutile.

(Defant and Drummond, 1990; Martin et al., 2005). Of course in such differentiated samples the role of accessory phases controlling the REE distribution should be taken into account and one could consider that the so called adakitic character is acquired due to fractional crystallization of accessory phases such as apatite or zircon. However, the HREE depletion is not only observed in the more felsic samples but in the less differentiated ones as well, thus demonstrating that this adakitic character is primitive and does not result of accessory phase crystallization. Again, for this kind of rocks, two petrogenetic models have been considered: (1) partial melting of the subducting oceanic crust (Defant and Drummond, 1990; Maury et al., 1996, Martin et al., 2005); and (2) partial melting of underplated mafic material (Kilian et al., 1995; Petford and Atherton, 1996; Arculus et al., 1999). In order to test these two hypotheses, the same modelling procedure as for the South Iliniza is followed. Major element mass balance between the basaltic compositions, residual

Table 8
Results for the mass balance calculations for the partial melting of the different considered sources in order to produce South Iliniza, Pilongo and Tishigcuchi parent magmas

	Source	Parent magma	ol %	opx %	cpx %	grt %	rt %	amp %	r^2	F
Mantle Sources	KLB-1	ILI 50	76.74	9.49	13.77				2.13	10.20
	KLB-1	ILI 50	60.40	20.18	13.89	5.53			2.03	2.30
	MP	ILI 50	67.38	21.22	11.40				2.73	12.10
	MP	ILI 50	46.45	34.30	11.82	7.43			2.54	1.30
Ocean basaltic sources	N-MORB	ILI 50			62.48	36.37	1.16		0.81	36.00
	N-MORBs	ILI 50			62.73	36.68	0.59		0.76	36.00
	E-MORBs	ILI 50			62.66	36.73	0.61		0.72	36.00
	GSC	ILI 50			66.41	32.24	1.34		0.49	36.00
	N-MORB	ILI 64			61.38	37.48	1.14		0.87	24.72
	N-MORBs	ILI 64			61.65	37.72	0.63		0.84	24.75
	E-MORBs	ILI 64			61.60	37.75	0.65		0.82	24.69
	E-MORBs	ILI 64			61.27	37.47	0.65	0.62	0.82	24.70
	GSC	ILI 64			64.81	33.93	1.25		0.42	24.93
	N-MORB	ILI 25			59.57	39.26	1.17		1.23	25.94
	N-MORBs	ILI 25			59.84	39.50	0.66		1.19	25.96
	E-MORBs	ILI 25			59.80	39.52	0.68		1.17	25.01
	GSC	ILI 25			63.02	35.69	1.29		0.67	26.18
Accreted crust	EAC	ILI 50			56.31	42.77	0.92		0.26	34.95
	EAC	ILI 64			56.19	42.92	0.89		0.57	24.09
	EAC	ILI 64			45.34	33.95	0.77	19.94	0.21	24.53
	EAC	ILI 25			54.26	44.81	0.93		0.44	25.40
	EAC	ILI 25			47.38	39.12	0.85	12.64	0.29	25.64
Metasomatized source	MDM15	ILI 1A	73.3	15.6	5.9	5.2			0.48	25.51

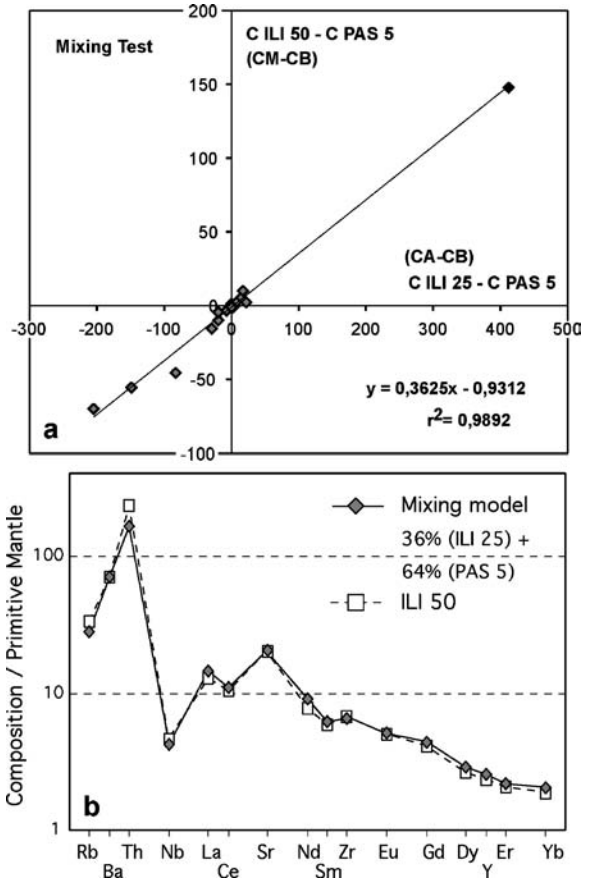


Fig. 6. (a) Mixing test to model the Iliniza Series parent magma (ILI 50). This test is based in the simple mixing equation: CM = X CA + (1 − X CA) CB. From this X CA = (CM − CB)/(CA − CB). Where: CM is the mixing resulting composition; CA and CB are respectively the acid and basic poles of the mixing; and X CA is the acid pole proportion in the mixing. In the graphic representation X CA is given by the mixing line slope. The validity of the test is done by the correlation coefficient (r^2). (b) Theoretical spidergram obtained by a model of magma mixing of 36% Pilongo Dome adakitic composition (ILI 25) plus 64% calc-alkaline Pasochoa Volcano (PAS 5) composition. Normalization to the primitive mantle of Sun and Mcdonough (1989).

mineral phases (Sen and Dunn, 1994; Table 7) and the rhyolitic sample ILI 64 (Table 2) predicts a degree of partial melting of about 24%, with a melting residue with an amphibole-bearing eclogite composition (Table 8). Trace element modelling was made using a batch melting process. In the La/Yb vs. La and La/Yb vs. Yb diagrams (Fig. 8) it can be seen that the rhyolites compositions may be reproduced by 8–10% partial melting of the N-MORB (Sun and Mcdonough, 1989) source, leaving an eclogitic residue. The other basaltic sources require a higher degree of melting (>35%), which lies out of the generally accepted values (Sen and Dunn, 1994; Rapp and Watson, 1995). Such 8–10% of melting degree obtained with a N-

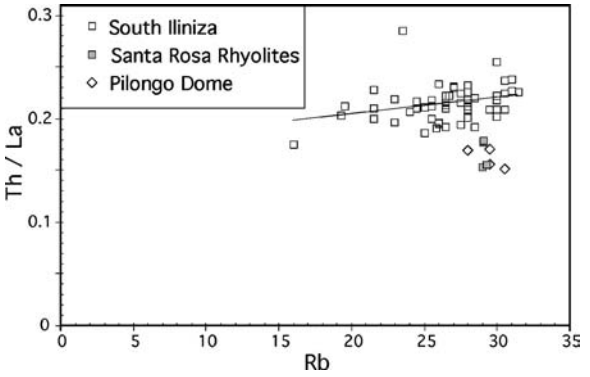


Fig. 7. Th/La vs. Rb diagram showing an almost horizontal linear trend for South Iliniza rocks. The Iliniza rhyolites as well as Pilongo rhyodacites lie out of this trend, indicating that a fractional crystallization process does not relate all these rocks.

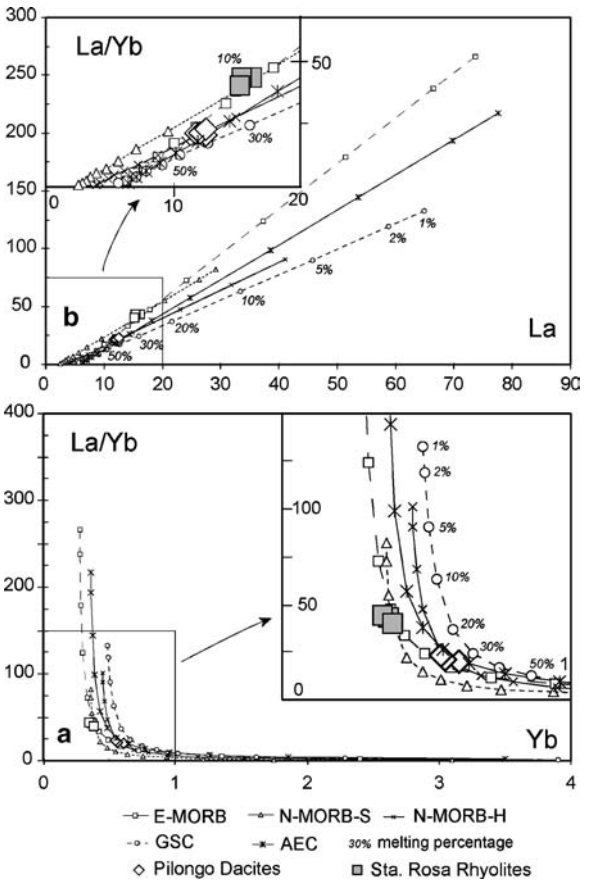


Fig. 8. Evolution of La/Yb vs. Yb (a) and La (b) obtained by a model of fractional melting of five different basaltic sources, leaving an eclogitic melting residue. N-MORB-H: 59.8% cpx + 39.5% grt + 0.7% rt (Hofmann, 1988); N-MORB-S: 59.8% cpx + 39.5% grt + 0.7% grt and E-MORB: 59;8% cpx + 39.5% grt + 0.7% rt (Sun and Mcdonough, 1989); GSC: 63% cpx + 35.7% grt + 1.3% rt (Verma and Schilling, 1982), and AEC: 54.3% cpx + 44.8% grt + 0.9% rt (Arculus et al., 1999). Ticks on the curves are percentages of partial melting.

MORB source is lower than the one obtained by the major elements mass balance calculation (24%). Nevertheless, this disagreement can be explained by a limited interaction between the upgoing slab melts and the mantle wedge. This process is able to change the major element compositions but it does not affect the trace elements contents, except for Ni and Cr and all other elements abundant in peridotites, which are enriched in the melt by interaction with the mantle peridotite (Rapp et al., 1999). Trace element composition of rhyolites is compared with the contents obtained by 10% and 24% batch partial melting of a N-MORB source, leaving an eclogitic residue (61.65% clinopyroxene+37.72% garnet+0.63% rutile) (Fig. 9). For HREE contents, the two models are able to reproduce the rhyolite composition, while for La, Ce and Sr the first model (10% batch melting) obviously shows a better fit. However, both models do not show a very good fit for LILE contents. This enrichment in Rb, Ba and K of the High SiO_2 adakitic rhyolites could either reflect variable extents of sea floor hydrothermal alteration of the basaltic crust (Rapp et al., 1999) or enrichment by hydrous fluids that must accompany slab melting (Grove et al., 2002).

7.4. Pilongo dome

As discussed before, this dome presents a very homogeneous composition, with a SiO_2 content of about 69% (samples ILI 25, 55A, 55B and 55C; Table 1). It can be considered as formed by a single, batch of highly evolved rhyodacitic magma arriving to the surface. In order to understand the genesis of this magma, a fractional crystallization process has been considered, taking into account the same parental magma as for the South Iliniza (ILI 50). However, as for the Iliniza adakitic rhyolites, the degrees of fractionation required to produce the Pilongo magmas are excessively high ($1-F>50\%$). In addition, in the diagram Th/La vs. Rb (Fig. 7), as for Iliniza rhyolites, Pilongo dome plots out of the sub horizontal trend defined by the Iliniza rocks, which precludes Pilongo magmas derivation by fractional crystallization from Iliniza magmas. Indeed, taking into account their marked high SiO_2 adakitic geochemical signature (Na_2O: 4.4–4.5 wt.%, Sr>450 ppm, La/Yb: 20.49–22.73 and Sr/Y: 58.2–62.2), melting of slab or underplated basalts appears as a realistic process. Consequently, as for Iliniza rhyolites, the same five basaltic source compositions were used to test this hypothesis (Table 8). The compositions of the residual mineral phases are taken from melting experiments of Sen and Dunn (1994) (Table 6). Based on this data set, Pilongo magmas could be generated by 26% partial melting of any of the considered basalts, leaving an eclogitic residue (Table 8). However, as shown in Fig. 8, the same model applied to trace elements (via batch melting) provides a good fit between calculation and analytical data, only when the source has a N-MORB composition (Hofmann, 1988). In this case the degree of melting obtained (20–30%) by major elements mass balance is in good agreement with that calculated with trace elements. This model implies that Pilongo magma did not undergo any significant kind of interaction with the mantle wedge during its transport towards the surface. There too, Rb, Ba and K contents appear higher in Pilongo rhyodacites than in calculated composition, a feature that has already been discussed for Iliniza Rhyolites. Consequently, it seems that Pilongo dome magmas were produced by partial melting (26%) of a N-MORB source (Hofmann, 1988). The absence of interaction with the mantle peridotite is quite surprising, but if the mantle wedge has already suffered an intense metasomatism by adakitic liquids before the ascension of Pilongo magmas, further interactions may had been prevented (Prouteau et al., 2001). Nevertheless, at this stage, given the absence of interactions, the partial melting of underplated basalts at the base of the crust can also be considered as a plausible model.

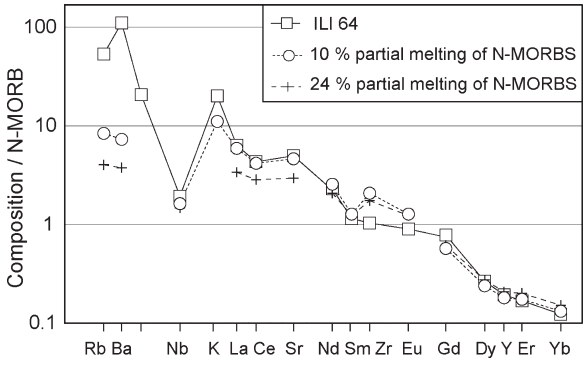


Fig. 9. N-MORB normalized spidergrams for 10% and 24% partial melting of a basaltic source (N-MORB after Sun and Mcdonough, 1989) compared to ILI 64 Iliniza rhyolite composition.

7.5. Tishigcuchi dome

Tishigcuchi lavas are homogeneous acid andesites (Table 2; Figs. 3 and 4). The homogeneity of these lavas led us to conclude that no important fractional crystallization processes participated into their evolution. When compared to North and South Iliniza, they are significantly enriched in MgO, K_2O, Rb, Ba, Th, Sr, Nb, La, Cr and Ni. Some of their characteristics such as low Y and Yb contents and high Sr contents point to an adakitic lineage. However, their low-SiO_2 content (59.8–62.3%), and

medium-K_2O (1.6%) as well as their high-LILE and transition element contents make them different from typical adakites. In fact, these characteristics are comparable (with a lesser enrichment in incompatible elements) to those of the high-K andesites found in Chimborazo volcano, located in the south of the Western Cordillera of Ecuador (Kilian et al., 1995), and to those of the Low Silica Adakites (LSA) of Martin et al. (2005), previously called high Mg#-andesites (Rapp et al., 1999). For Kilian et al. (1995), these characteristics are related to partial melting of an underplated basaltic crust. However, for Rapp et al. (1999) and Martin et al. (2005), some geochemical features of the LSA, as the low-Si and high-Mg, Cr, Ni contents, are typical of mantle peridotite melting whereas low-Y and Yb, and high-Sr contents testify that an adakitic component played a role in the genesis of these magmas. According to these two hypotheses, two models can be proposed:

(1) The first one considers the same parameters as for the Iliniza rhyolites and Pilongo rhyodacites with a basaltic accreted crust (EAC) as the source. As no mass balance equilibrium between the basaltic accreted crust and the Tishigcuchi compositions have been obtained, such hypothesis is discarded;

(2) The second model agrees with Rapp et al. (1999) and Martin et al. (2005) hypothesis and considers melting of a mantle peridotite previously metasomatized by slab melts.

The model for the genesis of Tishigcuchi magmas that best fit data considers the melting (F=10–13%) of a depleted mantle peridotite (Hofmann, 1988) previously metasomatized (15%) by an adakitic melt (ILI 25, Pilongo dome composition). The composition of this metasomatized source has been obtained by a simple mixing between a depleted mantle composition and the Pilongo adakite in 85:15 proportions (MDM15). Prouteau et al. (2001) showed that felsic melts are by far (more than 10 times) more efficient metasomatic agents than dehydration fluids, so the simple mixing between adakites and the mantle peridotite is justified.

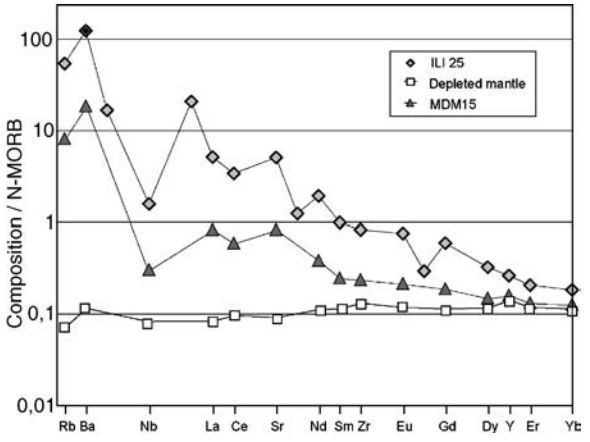


Fig. 10. Trace elements patterns for the adakitic-like lavas from Pilongo Dome (ILI 25), a depleted mantle composition (Hofmann, 1988) and the metasomatized source produced by the mixing of these two compositions (MDM15) in 15% and 85% respective proportions. Normalization to N-MORB Sun and Mcdonough (1989).

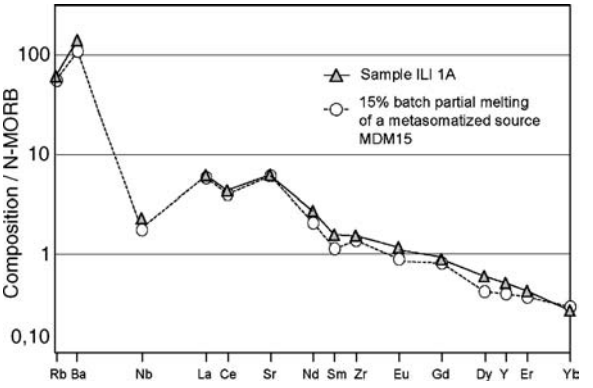


Fig. 11. Trace elements patterns for the composition produced by 13% batch partial melting of a metasomatized source (MDM15 of Fig. 11) compared to sample ILI 1A from Tishigcuchi Dome. Normalization to N-MORB of Sun and Mcdonough (1989).

The melting residue calculated by mass balance between the metasomatized source (MDM15) and ILI 1A comprise 73.3% olivine, 15.6% orthopyroxene, 5.9% clinopyroxene, 5.2% garnet and 1% magnetite (Table 8). Fig. 10 is a spider diagram that shows the compositions of the components taken into account for calculation of the metasomatized mantle peridotite MDM15. Fig. 11 shows that 13% of melting of such a metasomatized source well accounts for with Tishigcuchi lava composition.

8. Discussion

In subduction zones three main different sources can account for the origin of arc magmas: the mantle wedge metasomatized either by hydrous fluids (to produce calc-alkaline magmas) or silicate melts (to produce low-silica adakites), the subducted slab and the underplated basalts of the crust (to produce adakitic magmas). This study on IVC shows that at least the two first sources have been active (sometimes together) in order to generate the magmas of the whole complex. One of these sources is a mantle wedge peridotite previously metasomatized by a fluid-rich agent resulting of the subducted slab dehydration; the North Iliniza magmas

are generated through such a mechanism; the second mechanism is partial melting of subducted basalts, which is well exemplified by Pilongo Dome magma.

All other magma petrogenesis requires the involvement of these two end members through different kind of interactions:

(1) Magma-mixing: for instance, the South Iliniza parent magma composition appears to result from a magma mixing between two magmas: one with a calc-alkaline affinity (64%) and an adakitic rhyodacite (36%). This mixing between peridotite mantle melt and adakite may occur along magma pathways or in a subcrustal/crustal magma chamber. This process has also been proposed for the transitional adakites of Mount Cuernos in Negros Island (Sajona et al., 2000);

(2) Adakitic magma vs. peridotite: the Santa Rosa rhyolites appear to be generated by partial melting of basalts probably belonging to the subducting slab. However, due to their relatively high Mg, Ni and Cr contents (e.g. higher than those of Pilongo dome at higher silica contents), these adakitic melts are considered to have experienced a limited interaction with the mantle wedge peridotite during their ascent to the surface. Rapp et al. (1999) studied experimentally these kinds of interactions. These authors showed that when the adakitic melt/peridotite ratio is greater than 2, the adakitic melt is not totally consumed in metasomatic reactions with the mantle wedge, and part of this melt can reach the surface. However, due to these interactions, the uprising melt acquires some kind of mantle signature (high Mg, Ni and Cr), without losing its other slab melt characteristics;

(3) Melting of the mantle wedge peridotite metasomatized by slab melts: the Tishigcuchi acid andesite magmas appear to be generated by partial melting of mantle wedge previously metasomatized by an adakitic melt similar to Pilongo lava. Rapp et al. (1999) also showed that when the slab melt/peridotite ratio is low, all the slab-melt is entirely consumed in metasomatic reactions with the peridotite. It is the subsequent melting of this modified (slab melt metasomatized) mantle peridotite that gives rise to magmas such as Tishigcuchi andesites. Such a mechanism has also been proposed by Yogodzinski et al. (1994), in the Aleutian Arc and by Sajona et al. (2000) in the Negros Island (Philippines), and in Ecuador for the Antisana (Bourdon et al., 2003), Cayambe (Samaniego et al., 2005), and Mojanda–Fuya-Fuya (Robin et al., in press) volcanoes.

The point that appears peculiar to Ecuadorian arc is that all these mechanisms are represented not only in separated edifices of the volcanic arc, but also into a single long lived volcano. This situation is probably the result of the transitory situation of this arc. Indeed, if we consider the Gutscher et al. (2000) hypothesis, the Carnegie ridge entered in subduction a few My ago (6–8 My), resulting in the progressive decrease of the subduction angle and in a change of magma source for this volcanic arc. New magma sources, as the subducted basalts of the slab, are being activated whereas older ones (hydrous metasomatized mantle) are still active, leading to all kind of possible interactions between each other. However, in the IVC, these mantle vs. slab melts interactions could be chronologically ordered in a logical manner:

(1) Before the arrival of the Carnegie Ridge under the volcanic arc, production and differentiation of calc-alkaline magmas from the mantle wedge metasomatized by fluids (Pasochoa and North Iliniza magmas);

(2) When the Carnegie Ridge arrived under the volcanic arc (~100–120 km depth), it reached the PT conditions of its melting such that the production of adakitic magmas may begin, but in relatively small volumes, such that the slab melts are totally consumed in their interactions with the mantle wedge peridotite. Melting of this modified mantle wedge is at the origin of the Tishigcuchi magma;

(3) As progressively more Carnegie young basalts are implied in subduction, the volume of adakitic melts increases, such that they are not totally consumed in reaction with peridotite. Some of these adakites can directly reach the surface (Santa Rosa rhyolites and Pilongo), whereas other can mix with hydrous metasomatized mantle wedge melts, either along magmatic pathways in the mantle, in the MASH zone, or in crustal reservoirs (South Iliniza parental magma).

The age of entry of the Carnegie ridge into subduction is still a debated subject. Indeed based on different observations, a wide range of ages has been proposed by several authors. Spikings et al. (2001), suggest an age of 15 My for the arrival of the ridge into subduction; they consider that the high cooling and exhumation rates measured in the Cordillera Real and dated at 15 My are related to this event. Gutscher et al. (1999), studied the marine terraces uplift in the northern Ecuadorian coastal region, this uplift has an age of 8 My; which they interpret as the age of the beginning of the Carnegie ridge subduction under the continental margin. Bourdon et al. (2002b), estimated a minimum age of 5 My based on the adakitic imprint of the recent lavas from Pichincha Volcano. More recently, structural works carried out in the Ecuadorian coastal terraces suggest a Late Pliocene–Early Pleistocene age for uplift considered as due to the Carnegie Ridge arrival into subduction (Cantalamessa and Di Celma, 2004). Consequently a wide uncertainty remains about the moment when Carnegie ridge enters

in subduction, depending on authors this age ranges between 15 My and 2 My. Our work shows that a change in arc magma source occurred in recent times (may be less than 100 ky). In addition, in at least two other Ecuadorian volcanoes from the same arc, the Cayambe, in the eastern cordillera, and Pichincha in the western one, a similar chronology and change in magma source were also evidenced (Bourdon et al., 2002b; Samaniego et al., 2002; Bourdon et al., 2003; Samaniego et al., 2005). These authors pointed out to a progressive temporal change in magmatism from calc-alkaline to adakitic. Following these authors we propose to interpret the change in arc magma source under the IVC as reflecting the arrival of the Carnegie ridge under the volcanic arc. Assuming a constant subduction rate of the Nazca plate under South-America of about 5–6 cm/yr since Miocene (Pardo-Casas and Molnar, 1987; Trenkamp et al., 2002), it can be estimated that the time necessary for the Carnegie ridge to arrive under the volcanic arc after its entry in subduction is of about 5 My. This conclusion is consistent with the estimations of Bourdon et al. (2003).

It could also be considered that the mantle metasomatism is not a homogeneous process generalized to the whole mantle wedge. For instance, as proposed by Prouteau et al. (2001), magma is transferred during its ascent through conduits whose margins are progressively metasomatized by adakitic melts. When the whole conduit border is metasomatized, no more melt–peridotite interaction is allowed and consequently adakitic melts can reach the surface without important reactions with the mantle wedge peridotite. Such a situation would depend on the age of the conduit and new (not metasomatized) conduits can coexist with older (metasomatized) ones, thus allowing simultaneously different degree of melt–peridotite interactions.

It has also been suggested that some adakites may result through melting of basalts underplated beneath continental crust (Petford and Atherton, 1996; Kay, 1978; Petford and Gallagher, 2001; Garrison and Davidson, 2003). Nevertheless, high MgO, Cr and Ni concentrations in adakites have already been discussed and interpreted by several authors (Maury et al., 1996; Stern and Killian, 1996; Rapp et al., 1999; Smithies, 2000; Prouteau et al., 2001, Martin et al., 2005) as reflecting interactions between basalt melt and peridotite. In other words, these mantle peridotite/slab melt interactions implies that a peridotite slice existed above the source of adakites, condition which is realised if adakites are generated by subducted slab melting and precluded if adakites are produced by underplated basalts. As Ecuadorian adakites show evidences of interaction with peridotite it can be concluded that they are generated by slab melting rather than by underplated basalt melting. In addition, Weber et al. (2002) point out that no pervasive evidence of crustal melting has been found immediately in the south-western Colombia, concluding that the North-Andean magmas arise from the mantle wedge. This indicates that in Ecuador a mantle peridotite slice still exists over the subducted slab, which agrees with several recent works (Guillier et al., 2001; Bourdon et al., 2003).

Acknowledgments

Fieldwork support and/or stimulating discussions with Daniel Andrade, Diego Barba, César Witt, Erwan Bourdon, Pablo Samaniego, as the comments from Steve Weaver and an anonymous reviewer on a preliminary version of this work were very much appreciated and significantly improved this paper. Special thanks to Minard L. Hall for kindly providing some of the samples from Tishigcuchi dome. Marc Souris, Jorge Aguilar and the Instituto Geográfico Militar are deeply thanked for providing the data and to generate the Iliniza DEM. This work is part of S.H.'s PhD co-financed by the Ecuadorian "Fundación para la Ciencia y la Tecnología" (FUNDACYT), the Ambassade de France in Quito, the French "Institut de Recherche pour le Développement" (IRD) and the Departamento de Geofísica from the Escuela Politécnica Nacional (EPN) of Quito (Ecuador).

References

Arculus, R.J., Lapierre, H., Jaillard, E., 1999. Geochemical window into subduction and accretion processes: Raspas metamorphic complex, Ecuador. Geology 27, 547–550.

Bacon, C.R., Druitt, T.H., 1988. Compositional evolution of the zoned calcalkaline magma chamber of Mt. Mazama, Crater Lake, Oregon. Contrib. Mineral. Petrol. 98, 224–256.

Beate, B., Monzier, M., Spikings, R., Cotten, J., Silva, J., Bourdon, E., Eissen, J.P., 2001. Mio–Pliocene adakite generation related to flat subduction in southern Ecuador: the Quimsacocha volcanic center. Earth Planet. Sci. Lett. 192, 561–570.

Bourdon, E., 1999. Conséquences pétrogénétiques de la subduction d'une ride asismique: l'exemple du volcanisme de la marge équatorienne. Université de Bretagne Occidentale, Brest. 178 pp.

Bourdon, E., Eissen, J.P., Monzier, M., Robin, C., Martin, H., Cotten, J., Hall, M.L., 2002a. Adakite-like lavas from Antisana volcano (Ecuador): evidence for slab melt metasomatism beneath the Andean northern volcanic zone. J. Petrol. 43, 199–217.

Bourdon, E., Eissen, J.-P., Gutscher, M.-A., Monzier, M., Samaniego, P., Robin, C., Bollinger, C., Cotten, J., 2002b. Slab melting and slab melt metasomatism in the northern Andean volcanic zone: adakites and high-Mg andesites from Pichincha volcano (Ecuador). Bull. Soc. Géol. Fr. 173, 195–206.

Bourdon, E., Eissen, J.-P., Gutscher, M.-A., Monzier, M., Hall, M.L., Cotten, J., 2003. Magmatic response to early aseismic ridge

subduction: the Ecuadorian margin case (South America). Earth Planet. Sci. Lett. 205, 123–138.

Cantalamessa, G., Di Celma, C., 2004. Origin and chronology of Pleistocene marine terraces of Isla de la Plata and of flat, gently dipping surfaces of the southern coast of Cabo San Lorenzo (Manabí, Ecuador). J. South. Amer. Earth. Sci. 16, 633–648.

Clapperton, C.M., 1990. Glacial and volcanic geomorphology of the Chimborazo–Carihuairazo Massif, Ecuadorian Andes. Trans. R. Soc. Edinb. Earth Sci. 81, 91–116.

Cosma, L., Lapierre, H., Jaillard, E., Laubacher, G., Bosch, D., Desmet, A., Mamberti, M., Gabriele, P., 1998. Pétrographie et géochimie des unités magmatiques de la cordillère occidentale d'equateur (0°30′ S): implications tectoniques. Bull. Soc. Géol. Fr. 169, 739–751.

Cotten, J., Le Dez, A., Bau, M., Caroff, M., Maury, R.C., Dulski, P., Fourcade, S., Bohn, M., Brousse, R., 1995. Origin of anomalous rare-earth element and yttrium enrichments in subaerial exposed basalts: evidence from French Polynesia. Chem. Geol. 119, 115–138.

Defant, M.J., Drummond, M.S., 1990. Derivation of some modern arc magmas by melting of young subducted lithosphere. Nature (Lond.) 347, 662–665.

Defant, M.J., Jackson, T.E., Drummond, M.S., De Boer, J.Z., Bellon, H., Feigenson, M.D., Maury, R.C., Stewart, R.H., 1992. The geochemistry of young volcanism throughout western Panama and southeastern Costa Rica: an overview. J. Geol. Soc. (Lond.) 149, 569–579.

Drummond, M.S., Defant, M.J., 1990. A model for trondhjemite–tonalite–dacite genesis and crustal growth via slab melting: Archean to modern comparisons. J. Geophys. Res. 95, 21503–21521.

Fourcade, S., Allègre, C.J., 1981. Trace element behaviour in granite genesis: a case study — the calc-alkaline plutonic association from Quérigut complex (Pyrénées, France). Contrib. Mineral. Petrol. 76, 177–195.

Fujimaki, H., Tatsumoto, M., Aoki, K.-I., 1984. Partition coefficients of Hf, Zr, and REE between phenocrysts and groundmasses. J. Geophys. Res. 89, 662–672.

Garrison, J.M., et Davidson, J.P., 2003. Dubious case for slab melting in the Northern volcanic zone of the Andes. Geology 31 (6), 565–568.

Goosens, P.J., Rose, W., 1973. Chemical composition and age determination of tholeiitic rocks in the basic igneous complex, Ecuador. Geol. Soc. Amer. Bull. 84, 1043–1052.

Govindaraju, K., Roelandts, I., 1993. Second report on the first three GIT-IWG rock reference samples: anorthosite from Greenland, AN-G; Basalte d'Essey-la-côte, BE-N; Granite de Beauvoir, MA-N. Geostand. Newsl. 4, 49–138.

Green, T.H., 1994. Experimental studies of trace-element partitioning applicable to igneous petrogenesis – Sedona 16 years later. Chem. Geol. 117 (1–4), 1–36.

Grove, T.L., Parman, S.W., Bowring, S.A., Price, R.C., Baker, M. B., 2002. The role of an H_2O-rich fluid component in the generation of primitive basaltic andesites and andesites from the Mt. Shasta region, North California. Contrib. Mineral. Petrol. 142, 375–396.

Guillier, B., Chatelain, J.L., Jaillard, E., Yepes, H., Poupine, G., Fels, J.F., 2001. Seismological evidence on the geometry of the orogenic system in central-northern Ecuador (South America). Geophys. Res. Lett. 28, 3749–3752.

Gutscher, M.-A., Malavieille, J., Lallemand, S., Collot, J.-Y., 1999. Tectonic segmentation of the north Andean margin: impact of the Carnegie ridge collision. Earth Planet. Sci. Lett. 168, 255–270.

Gutscher, M.A., Maury, R., Eissen, J.P., Bourdon, E., 2000. Can slab melting be caused by flat subduction? Geology 28, 535–538.

Hall, M.L., Ramón, P., 1978. Estudio microsísmico del valle interandino entre Latacunga y Guayllabamba. Dirección Nacional de Defensa Civil, Quito, Ecuador, p. 29.

Hidalgo S., 2001. Estudio geovolcanológico del complejo volcánico Iliniza. Tesis de Grado, Escuela Politécnica Nacional, Quito, Ecuador, pp. 85.

Hidalgo, S., 2002. Géochimie du complexe volcanique des Iliniza: pétrogenèse de séries à affinité adakitique de l'arc équatorien. DEA Report. Université Blaise Pascal, Clermont-Ferrand, p. 50.

Hofmann, A.W., 1988. Chemical differentiation of the earth: the relationship between mantle, continental crust and oceanic crust. Earth Planet. Sci. Lett. 90, 297–314.

Hughes, R.A., 1998 — Mapa geológico de la cordillera occidental del Ecuador entre 0°–1°S. BGS-CODIGEM ed., Quito, Ecuador, 1/200 000.

Hughes, R.A., Pilatasig, L.F., 2002. Cretaceous and Tertiary terrane accretion in the Cordillera Occidental of the Andes of Ecuador. Tectonophysics 345, 29–48.

Kay, R.W., 1978. Aleutian magnesian andesites: melts from subducted Pacific Ocean crust. J. Volcanol. Geotherm. Res. 4, 117–132.

Kellogg, J.N., Ogujiofor, I.J., Kansaka, D.R., 1985. Cenozoic tectonics of the Panama and the north Andes blocks. Mem. Congr. Latinoamericano Geol. 6, 34–49.

Kepezhinskas, P.K., Defant, M.J., et Drummond, M.S., 1995. Na metasomatism in the island-arc mantle by slab melt-peridotite interaction: evidence from mantle xenoliths in the north Kamchatka arc. J. Petrol. 36 (6), 1505–1527.

Kilian, R., Hegner, E., Fortier, S., Satir, M., 1995. Magma evolution within the accretionary mafic basement of Quaternary Chimborazo and associated volcanoes (western Ecuador). Rev. Geol. Chile 22, 203–218.

Klein, M., Stosch, H.-G., Seck, H.A., Shimizu, N., 2000. Experimental partitioning of high field strength and rare earth elements between clinopyroxene and garnet in andesitic to tonalitic systems. Geochim. Cosmochim. Acta 64, 99–115.

Lagabrielle, Y., Moigne, J.L., Maury, R.C., Cotten, J., Bourgois, J., 1994. Volcanic record of the subduction of an active spreading ridge, Taitao peninsula (southern Chile). Geology 22, 515–518.

Leake, B.E., Woolley, A.R., Arps, C.E.S., Birch, W.D., Gilbert, M.C., Grice, J.D., Hawthorne, F.C., Kato, A., Kisch, H.J., Krivovichev, V.G., Linthout, K., Laird, J., Mandarino, J.A., Maresch, W.V., Nickel, E.H., Rock, N.M.S., Schumacher, J.C., Smith, D.C., Stephenson, N.C.N., Ungaretti, L., Whittaker, E.J.W., Guo, Y.Z., 1997. Nomenclature of amphiboles: report of the Subcommittee on Amphiboles of the International Mineralogical Association, Commission on New Minerals and Mineral Names. Mineral. Mag. 61, 295–321.

Lebrat, M., Mégard, F., Dupuy, C., Dostal, J., 1987. Geochemistry and tectonic setting of pre-collision cretaceous and Paleogene volcanic rocks of Ecuador. Geol. Soc. Amer. Bull. 99, 569–578.

Lonsdale, P., 1978. Ecuadorian subduction system. Am. Assoc. Pet. Geol. Bull. 62, 2454–2477.

Luhr, J.F., Carmichael, I.S.E., 1980. The Colima volcanic complex, Mexico. I: post-caldera andesites from Volcan Colima. Contrib. Mineral. Petrol. 71, 343–372.

Martin, H., 1987. Petrogenesis of archean trondhjemites, tonalites, and granodiorites from eastern Finland: major and trace element geochemistry. J. Petrol. 28, 921–953.

Martin, H., Smithies, R.H., Rapp, R., Moyen, J.-F., et Champion, D., 2005. An overview of adakite, tonalite-trondhjemite-granodiorite (TTG), and sanukitoid: relationships and some implications for crustal evolution. Lithos 79 (1–2), 1–24.

Maury, R.C., Sajona, F.G., Pubellier, M., Bellon, H., Defant, M.J., 1996. Fusion de la croûte océanique dans les zones de subduction/collision récentes: l'exemple de Mindanao (Philippines). Bull. Soc. Géol. Fr. 167, 579–595.

Monzier, M., Robin, C., Hall, M.L., Cotten, J., Mothes, P., Eissen, J.-P., Samaniego, P., 1997. Les adakites d'Equateur: modèle préliminaire. C. R. Acad. Sci. Paris 324, 545–552.

Morimoto, N., Fabries, J., Ferguson, A.K., Ginzburg, I.V., Ross, M., Seifert, F.A., Zussman, J., Aoki, K., Gottardi, G., 1988. Nomenclature of pyroxenes. Am. Mineral. 73, 1123–1133.

Morris, P.A., 1995. Slab melting as an explanation of Quaternary volcanism and seismicity in southwestern Japan. Geology 23, 395–398.

Pardo-Casas, F., et Molnar, P., 1987. Relative motion of the Nazca (Farallon) and South America plate since late Cretaceous time. Tectonics 6, 233–248.

Peacock, S.M., Rushmer, T., et Thompson, A.B., 1994. Partial melting of subducting oceanic crust. Earth Planet. Sci. Lett. 121 (1–2), 227–244.

Peccerillo, P., Taylor, S.R., 1976. Geochemistry of Eocene calc-alkaline volcanic rocks from the Kastamonu area, northern Turkey. Contrib. Mineral. Petrol. 58, 63–81.

Pennington, W.D., 1981. Subduction of the eastern Panama basin and seismotectonics of northwestern South America. J. Geophys. Res. 86, 10753–10770.

Petford, N., et Atherton, M., 1996. Na-rich partial melts from newly underplated basaltic crust: the Cordillera Blanca Batholith, Peru. J. Petrol. 37 (6), 1491–1521.

Petford, N., et Gallagher, K., 2001. Partial melting of mafic (amphibolitic) lower crust by periodic influx of basaltic magma. Earth Planet. Sci. Lett. 193 (3–4), 483–499.

Prévot, R., Chatelain, J.-L., Guillier, B., Yepes, H., 1996. Tomographie des Andes équatoriennes: évidence d'une continuité des Andes centrales. C. R. Acad. Sci. Paris 323, 833–840.

Prouteau, G., Scaillet, B., Pichavant, M., Maury, R.C., 2001. Evidence for mantle metasomatism by hydrous silicic melts derived from subducted oceanic crust. Nature (Lond.) 410, 197–200.

Rapp, R.P., Watson, E.B., 1995. Dehydration melting of metabasalt at 8–32 kbar: implications for continental growth and crust–mantle recycling. J. Petrol. 36, 891–931.

Rapp, R.P., Shimizu, N., Norman, M.D., Applegate, G.S., 1999. Reaction between slab-derived melts and peridotite in the mantle wedge: experimental constraints at 3.8 GPa. Chem. Geol. 160, 335–356.

Rayleigh, J., 1896. Theoretical considerations respecting the separation of gases by diffusion and similar processes. Philos. Mag. 42, 77–107.

Reynaud, C., Jaillard, E., Lapierre, H., Mamberti, M., Mascle, G., 1999. Oceanic plateau and island arcs of southwestern Ecuador: their place in the geodynamic evolution of northwestern South America. Tectonophysics 307, 235–254.

Ringwood, A.E., 1974. The petrological evolution of island arc systems. J. Geol. Soc. (Lond.) 130, 183–204.

Robin, C., Eissen, J.-P., Samaniego, P., Martin, H., Monzier, M., et Cotten, J., in press. From calc-alkaline to adakitic magmas at Late Pleistocene Mojanda - Fuya Fuya Volcanic complex (Ecuador). J. Petrol.

Rollinson, H.R., 1993. Using Geochemical Data: Evaluation, Presentation, Interpretation. Longman Group Limited, p. 351.

Sajona, F.G., Maury, R.C., Bellon, H., Cotten, J., Defant, M.J., Pubellier, M., 1993. Initiation of subduction and the generation of slab melts in western and eastern Mindanao, Philippines. Geology 21, 1007–1010.

Sajona, F.G., Maury, R.C., Bellon, H., Cotten, J., Defant, M., 1996. High field strength element enrichment of Pliocene–Pleistocene island arc basalts, Zamboanga peninsula, western Mindanao (Philippines). J. Petrol. 37, 693–726.

Sajona, F., Maury, R., Prouteau, G., Cotten, J., Schiano, P., Bellon, H., Fontaine, L., 2000. Slab melt as metasomatic agent in island arc magma sources, Negros and Bataan (Philippines). Isl. Arc 9, 472–486.

Samaniego P., 2001. Transition entre magmatismes calco-alcalin et adakitique dans le cas d'une subduction implicant une ride océanique : Le volcan Cayambe (Equateur). Ph.D, Université Blaise Pascal-Clermont-Ferrand 2, pp. 259.

Samaniego, P., Martin, H., Robin, C., Monzier, M., 2002. Transition from calc-alkalic to adakitic magmatism at Cayambe volcano, Ecuador: insights into slab melts and mantle wedge interactions. Geology 30, 967–970.

Samaniego, P., Martin, H., Monzier, M., Robin, C., Fornari, M., Eissen, J.P., et Cotten, J., 2005. Temporal evolution of magmatism at Northern Vocanic Zone of the Andes: the geology and petrology of Cayambe vocanic complex (Ecuador). J. Petrol. 46, 2225–2252.

Schmidt, M.W., Poli, S., 1998. Experimentally based water budget for dehydrating slabs and consequences for arc magma generation. Earth Planet. Sci. Lett. 163, 361–379.

Sen, C., Dunn, T., 1994. Dehydration melting of a basaltic composition amphibolite at 1.5 and 2.0 GPa: implications for the origin of adakites. Contrib. Mineral. Petrol. 117, 394–409.

Sigmarsson, O., Martin, H., Knowles, J., 1998. Melting of a subducting oceanic crust from U–Th disequilibria in austral Andean lavas. Nature (Lond.) 394, 566–569.

Smithies, R.H., 2000. The Archaean tonalite-trondhjemite-granodiorite (TTG) series is not an analogue of Cenozoic adakite. Earth Planet. Sci. Lett. 182, 115–125.

Soulas, J.-P., Egüez, A., Yepes, H., Pérez, V.H., 1991. Tectónica activa y riesgo sísmico en los Andes ecuatorianos y el extremo sur de Colombia. Bol. Geol. Ecuatoriano 2, 3–11.

Spikings, R.A., Winkler, W., Seward, D., Handler, R., 2001. Along-strike variations in the thermal and tectonic response of the continental Ecuadorian Andes to the collision with heterogeneous oceanic crust. Earth Planet. Sci. Lett. 186, 57–73.

Stern, C.R., Killian, R., 1996. Role of the subducted slab, mantle wedge and continental crust in the generation of adakites from the Andean austral volcanic zone. Contrib. Mineral. Petrol. 123, 263–281.

Stormer, J.C., Nicholls, J., 1978. Xlfrac: a program for the interactive testing of magmatic differentiation models. Comput. Geosci. 4, 143–159.

Sun, S.-S., Mcdonough, W.F., 1989. Chemical and isotopic systematics of oceanic basalts: implications for mantle composition and processes. In: Saunders, Norry (Eds.), Magmatism in the Ocean Basins. Geol. Soc. London Spec. Pub., vol. 42, pp. 313–345.

Tatsumi, Y., 1986. Formation of volcanic front in subduction zones. Geophys. Res. Lett. 13, 717–720.

Tatsumi, Y., 1989. Migration of fluid phases and genesis of basalt magmas in subduction zones. J. Geophys. Res. 94, 4697–4707.

Tatsumi, Y., Eggins, S., 1995. Subduction zone magmatism. Blackwell Science, Cambridge, USA, p. 221.

Tatsumi, Y., Kogiso, T., 1997. Trace element transport during dehydration processes in the subducted oceanic crust 2. Origin of chemical and physical characteristics in arc magmatism. Earth Planet. Sci. Lett. 148, 207–221.

Trenkamp, R., Kellogg, J.N., Freymueller, J.T., Mora, H.P., 2002. Wide plate margin deformation, southern Central America and

northwestern South America, CASA GPS observations. J. South Amer. Earth Sci. 15, 157–171.

Verma, S.P., Schilling, J.-G., 1982. Galapagos hotspot-spreading center system — 2. $^{87}Sr/^{86}Sr$ and large ion lithophile element variations (85°W–101°W). J. Geophys. Res. 87, 10838–10856.

Weber, M.B.I., Tarney, J., Kempton, P.D., et Kent, R.W., 2002. Crustal make-up of northern Andes: evidence based on deep crustal xenolith suite Mercaderes, SW Colombia. Tectonophysics 354 (1–4), 49–82.

Wyllie, P.J., Sekine, T., 1982. The formation of mantle phlogopite in subduction zone hybridization. Contrib. Mineral. Petrol. 79, 375–380.

Yogodzinski, G.M., Volynets, O.N., Koloskov, A.V., Seliverstov, N.I., Matvenkov, V.V., 1994. Magnesian andesites and the subduction component in a strongly calc-alkaline series at Piip volcano, far western Aleutians. J. Petrol. 35, 163–204.

Yogodzinski, G.M., Lees, J.M., Churikova, T.G., Dorendorf, F., Woerner, G., Volynets, O.N., 2001. Geochemical evidence for the melting of subducting oceanic lithosphere at plate edges. Nature (Lond.) 409, 500–504.

Zamora, D., 2000. Fusion de la croûte océanique subductée: approche expérimentale et géochimique. Université Thesis, Université Blaise Pascal, Clermont-Ferrand, 314 pp.